

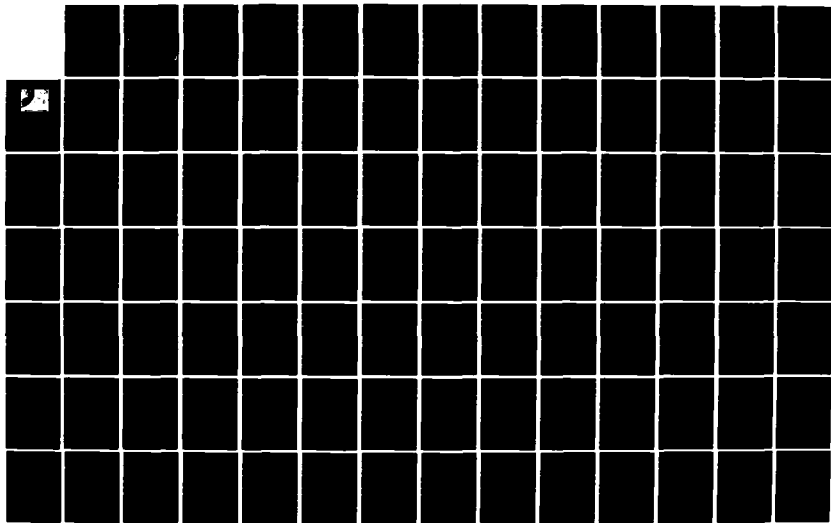
AD-A151 893

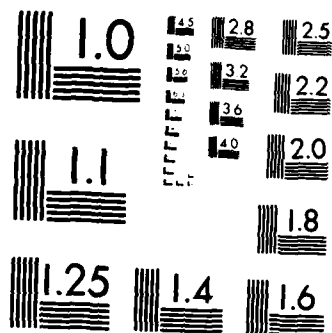
THE EFFECTS OF WATER AND HYDROGEN ON MATERIALS USED IN  
INTEGRATED CIRCUIT PACKAGES(U) AIR FORCE INST OF TECH  
WRIGHT-PATTERSON AFB OH SCHOOL OF ENGI. M W PRAIRIE  
DEC 84 AFIT/GE/ENG/84D-51 F/G 11/9

1/2

UNCLASSIFIED

NL





MICROCOPY RESOLUTION TEST CHART  
NATIONAL BUREAU OF STANDARDS 1963-A

AD-A151 893

DTIC FILE COPY



THE EFFECTS OF WATER AND HYDROGEN ON MATERIALS  
USED IN INTEGRATED CIRCUIT PACKAGES

THESIS

Michael W. Prairie  
Second Lieutenant, USAF

AFIT/GE/ENG/84D-51

This document has been approved  
for public release and sale; its  
distribution is unlimited.

DEPARTMENT OF THE AIR FORCE  
AIR UNIVERSITY

**AIR FORCE INSTITUTE OF TECHNOLOGY**

Wright-Patterson Air Force Base, Ohio

85 03 13 078

DTIC  
ELECTE  
APR 02 1985  
S D E

AFIT/GE/ENG/84D-51

THE EFFECTS OF WATER AND HYDROGEN ON MATERIALS  
USED IN INTEGRATED CIRCUIT PACKAGES

THESIS

Michael W. Prairie  
Second Lieutenant, USAF

AFIT/GE/ENG/84D-51

IC  
CTE  
O 2 1985  
E D

ALL INFORMATION CONTAINED  
HEREIN IS UNCLASSIFIED  
DATE 10-10-80 BY 10430

AFIT/GE/ENG/84D-51

THE EFFECTS OF WATER VAPOR AND HYDROGEN ON  
MATERIALS USED IN INTEGRATED  
CIRCUIT PACKAGES

THESIS

Presented to the Faculty of the School of Engineering  
of the Air Force Institute of Technology

Air University

In Partial Fulfillment of the  
Requirements for the Degree of  
Master of Science in Electrical Engineering

Michael W. Prairie, B.S.E.E.  
Second Lieutenant, USAF

December 1984

Accession For	
NTIS GRA&I	<input checked="checked" type="checkbox"/>
DTIC TAB	<input type="checkbox"/>
Unannounced	<input type="checkbox"/>
Justification	
By	
Distribution/	
Availability Codes	
Avail and/or	
Proc	
A-1	

Approved for public release; distribution unlimited.



## Preface

The purpose of this study was to analyze the material properties of some of the many materials used in packaging integrated circuits. Although I am an electrical engineer, I feel that this study of a related subject, in the field of material science, has broadened my knowledge base in the field of microelectronics. It has also given me appreciation for the problems that must be solved in order to get the electronics into a useable form.

The completion of this thesis was no easy task, and I sincerely doubt that I could have completed all the work involved without the help of many others. I would like to thank my thesis committee, Capt Donald R. Kitchen for his untiring guidance and support, and Capt Dale Hibner for assistance in writing this document. I would also like to thank Dr. Robert W. Thomas of the Product Evaluation Section of the Reliability and Compatability Division of the Rome Air Development Center for his cooperation in the use of the lab. I would like to extend a word of thanks to the personnel at the lab for their cooperation and support, especially 1Lt Amy Potts who assisted me with the operation of the equipment required for the study.

Finally, I wish to thank Sharron for her concern and support, editorial as well as emotional, throughout this entire ordeal.

Michael W. Prairie

## Table of Contents

	Page
Preface . . . . .	ii
List of Figures . . . . .	v
List of Tables . . . . .	viii
Abstract . . . . .	ix
I. Introduction . . . . .	I-1
Background . . . . .	-1
Problem Statement . . . . .	-2
Scope . . . . .	-4
Approach and Presentation . . . . .	-5
Major Results . . . . .	-6
II. Adsorption and Desorption in Determining Solid Surface Characteristics . . . . .	II-1
Adsorption and Desorption Phenomena . . . . .	-1
Sorption Measurement Techniques . . . . .	-6
Vacuum Microbalance Design . . . . .	-10
Microgravimetric Studies with Residual Gas Analysis . . . . .	-15
Errors in Microgravimetric Analysis . . . . .	-19
III. Adsorption Study of Materials . . . . .	III-1
Equipment Used . . . . .	-1
Polyimide Adsorption Experiment . . . . .	-6
Gold Adsorption Study . . . . .	-12
Nickel Adsorption Study . . . . .	-15
IV. Results and Discussion . . . . .	IV-1
RC-5878 Polyimide Adsorption Study . . . . .	-1
Gold Adsorption Study . . . . .	-4
Nickel Adsorption Study . . . . .	-4
V. Conclusions and Recommendations . . . . .	V-1
Inferences from the Results . . . . .	-1
Recommendations for Further Studies . . . . .	-2
Appendix A: Microbalance Calibration . . . . .	A-1
Appendix B: Microbalance Operation . . . . .	B-1

Appendix C: Proposed Digital Controller . . . . .	C-1
Appendix D: BET Surface Area Measurement . . . . .	D-1
Appendix E: Microbalance Parts Legend . . . . .	E-1
Bibliography . . . . .	BIB-1



## List of Figures

Figure	Page
I-1. Corrosion on a Bond Pad due to Moisture in the Integrated Circuit Package (mag- nified 1800X) . . . . .	I-2
II-1. Change of Potential Energy for Activated Adsorption . . . . .	II-2
II-2. Classification of the Principal Types of Isotherms According to Brunauer, Deming, Deming and Teller . . . . .	II-3
II-3. Comparison Plots Based on Standard Isotherms . . . . .	II-5
II-4. Beam Microbalance of Symmetrical Design with a Trussed Beam and Magnetic Compensation . . . . .	II-9
II-5. Microbalance with Automatic Compensating Network . . . . .	II-13
II-6. Schematic of the Principal Parts of a Residual Gas Analyzer . . . . .	II-18
II-7. Mass Spectrum of the Cracking Patterns of Four Commonly Observed Gases . . . . .	II-19
II-8. Illustration of Apparent Mass Changes Caused by Thermomolecular Flow . . . . .	II-23
II-9. Longitudinal Knudsen Forces Caused by Thermomolecular Flow . . . . .	II-23
II-10. Opposing Forces Acting on a Symmetrical Microbalance . . . . .	II-24
III-1. Ultragravimetric and Residual Gas Analyzer Apparatus for Studying Samples Loaded from a Controlled Environment . . . . .	III-2
III-2. Dual-path Light Source and Photo- detectors Symmetrically Located on Either Side of the Pivot . . . . .	III-4
III-3. Typical RGA Spectrum of the Polyimide Film During the Cure Cycle . . . . .	III-8

III-4.	Water Adsorption on Polyimide Sample RC-1 . . . . .	III-9
III-5.	Water Adsorption on Polyimide Sample RC-2 . . . . .	III-10
III-6.	Water Adsorption Isotherm on Polyimide Sample RC-3 . . . . .	III-11
III-7.	Sample Configuration for Gold Adsorption Study . . . . .	III-13
III-8.	Results from the Water Adsorption on Gold Foil . . . . .	III-15
III-9.	Auger Analysis of Nickel Foil after Sputtering for 20 Minutes . . . . .	III-17
III-10.	RGA Spectrum of Hydrogen Exposure to Dry Nickel Sample in the Stainless Steel Microbalance . . . . .	III-18
III-11.	Isotherm of Water Adsorption on Nickel Foil . . . . .	III-19
III-12.	Correction for Pressure Meter Calibrated for Nitrogen . . . . .	III-22
IV-1.	Isotherms of Water Adsorption on RC-5878 Polyimide Samples RC-1, RC-2 and RC-3, Normalized to 100 Square Centimeters Surface Area . . . . .	IV-2
IV-2.	BET Plot of RC-3 Adsorption Isotherm for BET Surface Area Analysis . . . . .	IV-3
IV-3.	Auger Scan of Nickel Foil Before Sputtering . . . . .	IV-5
IV-4.	Isotherms of Water Adsorption on Nickel Foil . . . . .	IV-7
IV-5.	BET Plots of Figure IV-4 for BET Surface Area Analysis . . . . .	IV-7
IV-6.	Hydrogen Exposure to Nickel Surface with Monolayer Water Molecule Coverage . . . . .	IV-9
A-1.	Calibration Curve for Buoyancy Bulb in Nitrogen . . . . .	A-4

A-2.	Calibration Curve for Tantalum Weight in Nitrogen . . . . .	A-4
B-1.	Schematic for Analog Microbalance Controller . . . . .	B-4
C-1.	Proposed Digital Microbalance Controller . . . . .	C-4
D-1.	Adsorption Isotherm of Nitrogen Adsorbed on Silver Powder . . . . .	D-1
D-2.	BET Plot of Nitrogen Adsorbed on Silver Powder . . . . .	D-4

## List of Tables

Table	Page
III-1. Cure Cycles for Each Polyimide Sample Tested . . . . .	III-8
III-2. Data Points Taken for the Water Adsorption on Nickel . . . . .	III-20
III-3. Pressure Increases in Hydrogen with Corresponding Mass Changes . . . . .	III-22
A-1. Calibration Using the Buoyancy Bulb . . . . .	A-1
A-2. Calibration Run Using the Tantalum Weight . . . . .	A-2

Abstract

This investigation determined the adsorption properties of water on RC-5878 polyimide, rolled gold foil, and rolled nickel foil at 20°C, as well as the effects that hydrogen has on nickel foil with a monolayer coverage of water molecules. Adsorption isotherms were obtained using a vacuum ultramicrobalance with a sensibility of 0.1 micrograms per 10 gram load. The microbalance system includes a gas handling system, a stainless steel housing, and a quadrupole residual gas analyzer. The isotherms were analyzed using the B. E. T. surface area technique.

The results showed that RC-5878 polyimide adsorbs water in an amount proportional to the thickness of the sample when the given cure is used. The rolled gold foil showed no mass gain from water adsorption. The nickel foil adsorbed water on 0.86 cm<sup>2</sup> of the 210 cm<sup>2</sup> sample, and adsorbed on 0.40 cm<sup>2</sup> during the second run of the experiment. An Auger scan revealed a large concentration of oxygen due to nickel oxide, which acted as a passivation layer for the remaining nickel sample surface. A monolayer of water molecules was obtained on the nickel surface, and hydrogen was admitted to the system. The sample exhibited a mass gain which was attributed to hydrogen bonding on the nickel oxide surface.

## I. INTRODUCTION

### Background

In the field of integrated circuits, controlling ambient contaminants during fabrication is becoming more important, especially with the small geometries that exists today. Water is one such contaminant that causes circuit failure in hermetically sealed integrated circuit packages (28:711). The assumption is that water, as well as other impurities, is adsorbed onto the surface of the packaging materials before they are used. When the package is sealed, the water is trapped inside where it can corrode, crack or short out the circuit. Figure I-1 shows such a problem, where moisture caused a contact pad to corrode.

In order to increase the reliability of these circuits, such surface reaction problems must be solved, but more has to be learned about the reactions taking place at the surface of the materials. By studying the materials used and their reactions with controlled ambients, knowledge will be gained that could ultimately be useful in producing more reliable integrated circuits.

The analysis of the adsorption of gases and vapors on solids provides information such as rates of adsorption and adsorption isotherms, which can be used to make deductions about the chemistry and physics of the surface of the solid

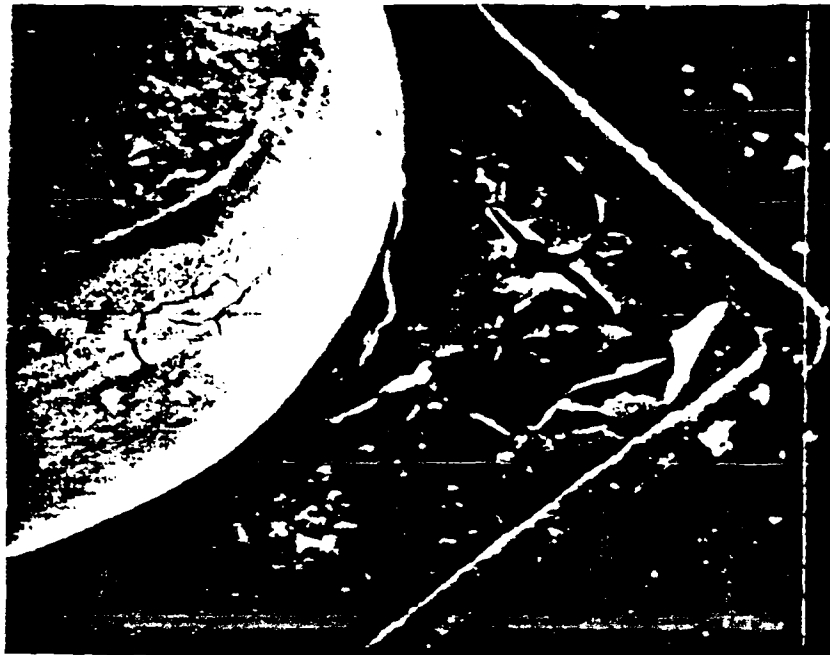


Figure I-1. Corrosion on a Bond Pad due to Moisture in the Integrated circuit Package (magnified 1800X).

(16)

(27:209). When this is known, techniques for assembling integrated circuit packages can be enhanced so that the contamination from impurities in the ambient can be decreased or eliminated.

#### Problem Statement

The first step toward raising the reliability of integrated circuits through better packaging techniques is to learn more about the adsorption properties of ambients on packaging materials. The objective of this research is

to determine the adsorption characteristics of Dupont RC-5878 polyimide, gold, and nickel. The test ambients were limited to hydrogen and to water, because they are common and present major problems to the semiconductor industry.

Major Equipment. The major apparatus chosen for the study is a stainless-steel, ultra-high vacuum system which incorporates an ultramicrogravimetric vacuum microbalance and a residual gas analyzer. The microbalance has a 20 g load capacity and has a sensitivity of 0.1 microgram for a 10 gram load. Mass changes are recorded while simultaneously monitoring the composition of the residual gas with the UTI quadrupole gas analyzer, located in line-of-sight to the sample to eliminate secondary surface reactions. The data collected reveals the quantity and composition of the adsorbed and desorbed products of the experiments.

Approach. There are three major parts to the study. The first part was the familiarization of the equipment by performing tests on previously tested materials. Also, the possibility of digitizing the control system was investigated to make the response times faster while increasing the accuracy of the data. These results are included in Appendix C.

The second step was to perform the tests on the samples. The samples were loaded into the system and the chamber was evacuated to the desired base pressure. The



samples were then exposed to water vapor at different partial pressures in order to construct isotherms, from which useful data could be obtained. Furthermore, The nickel sample was exposed to hydrogen before and after water was adsorbed onto the surface to determine if the hydrogen displaced the water.

The final step in this research was to document the findings of the investigation and draw conclusions from the data concerning the existence of adsorption and any reactions taking place on the surface. Recommendations for further study were then made.

#### Scope

The scope of this research is limited to the determination of the adsorption properties of water vapor on a polyimide, gold and nickel, including the effects of hydrogen on the water adsorbed onto the nickel surface. The equipment used was an ultramicrogravimetric vacuum microbalance to measure changes in mass due to adsorption or desorption, coupled with a mass spectrometer to analyze the outgassed products of the reactions. The samples were tested as described in the problem statement.

This research does not attempt to determine the adsorption properties of other materials, such as ceramics, metal alloys and sealing glasses, used in packaging integrated circuits. Also, it does not attempt to

determine the actual chemical reactions during adsorption and desorption, just that they do occur on the materials tested at the specified rates and quantities. These tasks are left to the chemists and those who have an interest in finding the properties of other materials.

#### Approach and Presentation

This thesis research is presented in the following chronological order. There are four main sections; the review of the literature, the adsorption study, the discussion of the results, and the conclusions.

Chapter II presents the theories used in this research from the literature. Section II-1 discusses the theory of adsorption and desorption and how the data can be used to determine surface characteristics. Section II-2 discusses the theory and the operation of a microgravimetric system, including a discussion of the possible errors in such a system.

The next section, chapter III, discusses the experiment itself. Section III-1 presents a discussion of the equipment used in the experiment. Section III-2 presents the procedures that were followed for the experiments, as well as the data that was compiled from the tests performed on each sample.

Chapter IV presents the results of the adsorption experiments. The results of each experiment are presented

and the reasons for them are discussed. Chapter V presents the conclusions drawn from the results in Chapter IV, and offers recommendations for further study.

Finally, the appendices contain supplemental information that is needed for understanding the material in this report. Appendix A contains the data used in calibrating the microbalance. Appendix B discusses the operation of the analog controller, while Appendix C offers some ideas on digitizing that controller. Appendix D presents the BET (Brunauer, Emmett and Teller) method for finding the surface area of a sample from adsorption data.

### Major Results

The major result of the thesis research on the Dupont RC-5878 polyimide is that it does adsorb water vapor, given the recommended cure. The data shows that the polyimide samples tested adsorbed water vapor at 20°C, and the thickness of the sample was directly related to the amount of water adsorbed.

The rolled gold foil sample tested did not adsorb water onto the surface at 20°C. The data showed that there was no mass gain due to water adsorption when exposed to water vapor, so the gold could be used in the nickel adsorption experiment without altering the results.

There are two results from the nickel adsorption study. First, water vapor does adsorb on nickel foil at

20°C, but only on a small part of the total surface, probably due to the passivation of the rest of the surface by nickel oxide. The second result is the sample gained mass when a monolayer of water molecules was exposed to hydrogen, instead of the expected mass loss due to a displacement reaction between  $H_2$  molecules and heavier  $H_2O$  molecules.

## II. ADSORPTION AND DESORPTION IN DETERMINING SOLID SURFACE CHARACTERISTICS

### Adsorption and Desorption Phenomena

Description. Adsorption is the assimilation of molecules from a gas or vapor ambient onto the surface of a solid in that ambient. Physical adsorption (physisorption) is characterized by the release of reaction heat on the order of the condensation heat of the gas or vapor during adsorption. Since this is true, the heat of adsorption is on the order of the heat of vaporization, so the adsorbate can be desorbed almost completely by lowering the pressure of the gas (17:127).

Some of the quantitative parameters for an activated adsorption process are: the equilibrium distance of the adsorbate from the surface,  $r_0$ ; the isotheric heat of adsorption,  $q$ ; the activation energy for desorption,  $E_D$ , and the activation energy for adsorption,  $E_A$ . These parameters are depicted in Figure II-1. When the gas and solid are separated by an infinite distance, the potential energy is defined as zero and is taken to be the potential energy reference (6:394).

The binding of the molecules of the adsorbate on the surface of the solid are caused by dispersion forces known as van der Waals forces (17:127). Henderson and Snook (14:2956) have developed van der Waals theory of adsorption

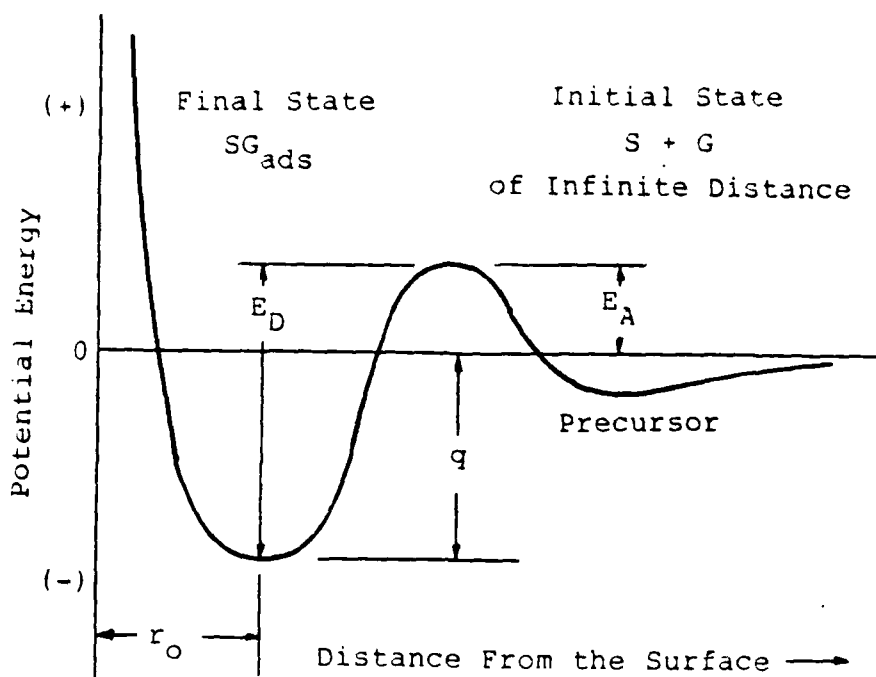


Figure II-1. Change of Potential Energy for Activated Adsorption. (6:394)

in great mathematical detail.

Adsorption studies can provide a great deal of information, but three fundamental questions must be answered first. These questions are: what are the adsorbed species, what is the relative population, and where are they located on the surface (6:390)? Depending on the method used in collecting the data, the answers can be measured directly. Otherwise they can be calculated or inferred from the results.

Deductions about the physics and chemistry of the solid surface can be made from data measured directly, such as rates of adsorption, but often require data in the form of an isotherm or isobar (27:210). At equilibrium, the mass of the adsorbate per unit mass of the adsorbent is a function of pressure and temperature alone, where the adsorbate is the adsorbed gas and the adsorbent is the solid. By holding the temperature constant and measuring the mass while varying the pressure, isotherms can be readily determined (6:395).

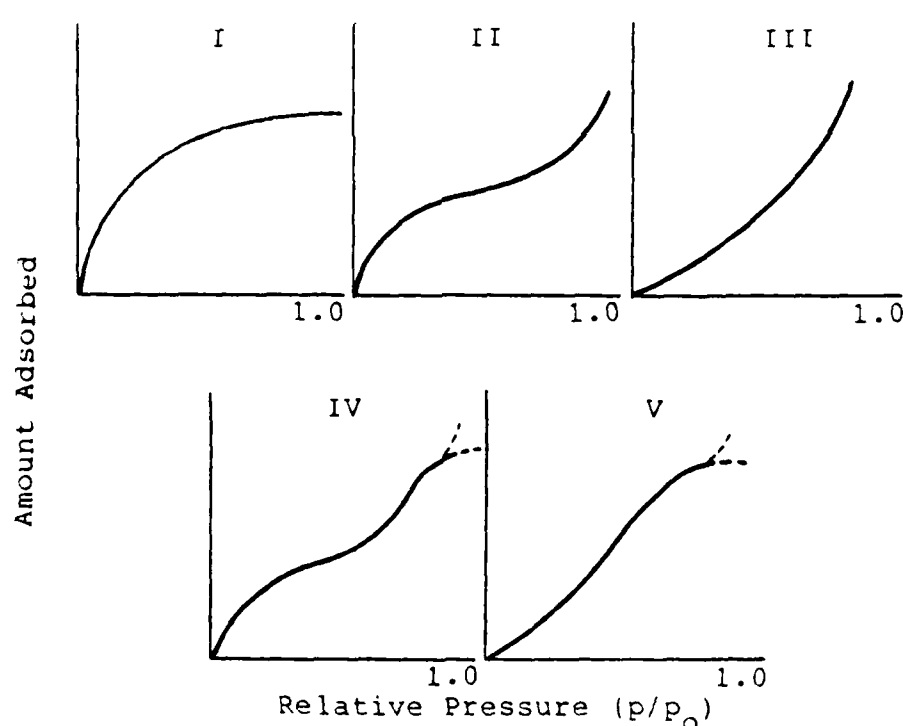


Figure II-2. Classification of the Principal Types of Isotherms According to Brunauer, Deming, Deming and Teller. (4:544)

Isotherms. The information that can be deduced from isotherms include adsorption heats and entropies at the gas-solid interface, adsorptivity and adsorption kinetics of the adsorbent, surface area and texture of the solid, and pore size and distribution at the surface (20:1558; 17:128). These adsorption isotherms can be classified into five types, known as the BET (Brunauer, Emmett, Teller) or BDDT (Brunauer, Deming, Deming, and Teller) classification (4:543). These principal types of isotherms are shown in Figure II-2.

The type I isotherm indicates that the surface has micropores, less than 2 nm in diameter by Durbin's classification. Adsorbed molecules in the pores are attracted by more than one surface at a time, so the enthalpy is high at lower partial pressures. At higher partial pressures, the pores are full, and since multilayer condensation does not occur, the isotherm reaches equilibrium (4:544).

The type II isotherm is the most common type and is modeled by the classical BET equation (see Appendix D). Though the BET equation has been criticized, it has been applied to many isotherms, and has provided information for finding the monolayer coverage and, ultimately, the surface area (4:543). In practice, the BET equation has been found to be accurate only in the dimensionless pressure ( $p/p_0$ ) range of 0.05 to 0.35 (4:544). The BET method of



determining the surface area is outlined by Robens (17:159), and is presented in Appendix D.

When the interaction between the gas and solid is low at low partial pressures and higher at higher partial pressures, the isotherm produced is a type III (or V) with the initial concave curve (4:544). A type IV or V isotherm is produced when mesopores (2-20 nm) or macropores (>20 nm) exist on the surface. These arise from capillary condensation in the pores. These isotherms generally contain a hysteresis loop at the end which contains information about the pore size and distribution (4:545).

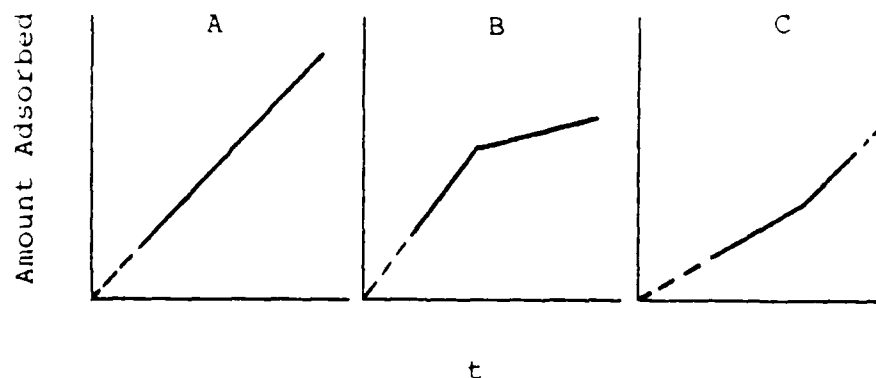


Figure II-3. Comparison Plots Based on Standard Isotherms: (a) Non-porous Sample, (b) Sample Containing Micropores, (c) Sample Containing Mesopores. (4:544)

Comparison plots can be used to determine the texture of the surface. By assuming a standard isotherm for a particular adsorbent on a non-porous surface, and plotting

it against that of an unknown sample surface, the plot will take the form of one of the plots shown in Figure II-3. If the surfaces match, then the plot will look like the first one. For a surface with a large number of micropores, the plot will look like the second, and mesopores will yield the third (4:544).

#### Sorption Measurement Techniques

There are several methods for obtaining sorption data, but the three most widely known methods for obtaining isotherms are continuous flow, volumetric, and gravimetric techniques (20:1558). Whether it be monitoring pressure changes to determine the number of molecules adsorbed, or monitoring the mass change, any experimental technique that is related to the molecules adsorbed or desorbed is a suitable method (7:130).

Continuous Flow. The continuous flow method consists of a gas that flows over the sample and is analyzed to find how much adsorbate has left the mixture. The gas phase is a mixture of the adsorbate and an inert gas. As the gas passes over the sample, the adsorbate is removed from the mixture in some quantity, and the change in the gas composition is detected by a thermal sensor. This method is advantageous because a high vacuum is not required, and it is an easy way to determine the surface area of the sample (20:1558).

Volumetric. The volumetric technique for obtaining isotherms requires accurate pressure measurements before and after a known quantity of gas is admitted to the chamber. Assuming that there is no adsorption onto the walls of the chamber, the difference measured in the pressure is related to the amount of adsorbate taken up by the sample. This method is good with the use of inert gases, but is poor when reactive gases are used because of the changes in pressure due to the reactions between the gases. Another disadvantage is that the detection of irreversible sorption is practically impossible (20:1558).

Gravimetric. The gravimetric technique consists of a sample loaded into gravimetric balance which allows adsorbates to be admitted and evacuated. The mass change of the sample is measured directly as is pressure, both of which are measured independently (20:1558). Although the method is tedious and time consuming, the quality and quantity of the data is superior to that of volumetric studies (6:420). Because the mass changes are measured directly, the equilibrium points are readily apparent, while other methods require corrections in the data and have calibration constraints (4:545).

The type III isotherm usually describes gases that condense at room temperature, and is best found using gravimetric techniques (4:545). Monitoring mass changes in time using a microbalance is a common method for obtaining

oxidation kinetics, as well as the degradation of resins and adsorption on catalysts (15:397; 22:2444). A suitable pressure range for thermogravimetric analysis is between 0.1 Torr and 760 Torr (21:138). Hussey, et al. reported use of a vacuum microbalance for oxidation kinetics of metals, with a pressure range of  $10^{-6}$  to 760 Torr and a maximum temperature of 1100 °C. The noise level of the system was reported as approximately 3 micrograms (15:399).

Microbalances. There are three types of microbalances, the spiral or helices, torsion, and the pivotal beam balance. The quartz helices of the spiral balance are very delicate and easily broken. They are also susceptible to oscillations resulting from poor shock mounting (8:1206). This is understandable since they work on the principal of measuring the deflection of a fine quartz spring. The extension of the spring is proportional to the mass, and obeys Hooke's law (11:9).

The torsion balance consists of a beam that is suspended by a primary fulcrum that is usually a quartz or tungsten wire. A small moment in the wire is used to detect mass changes (11:13). The major disadvantages of this type of balance is that it is sensitive to shocks and requires frequent calibration (8:1206).

The pivotal beam balance, shown in Figure II-4, consists of a beam resting on a fulcrum of two points (11:15). One side of the beam holds the sample, and the

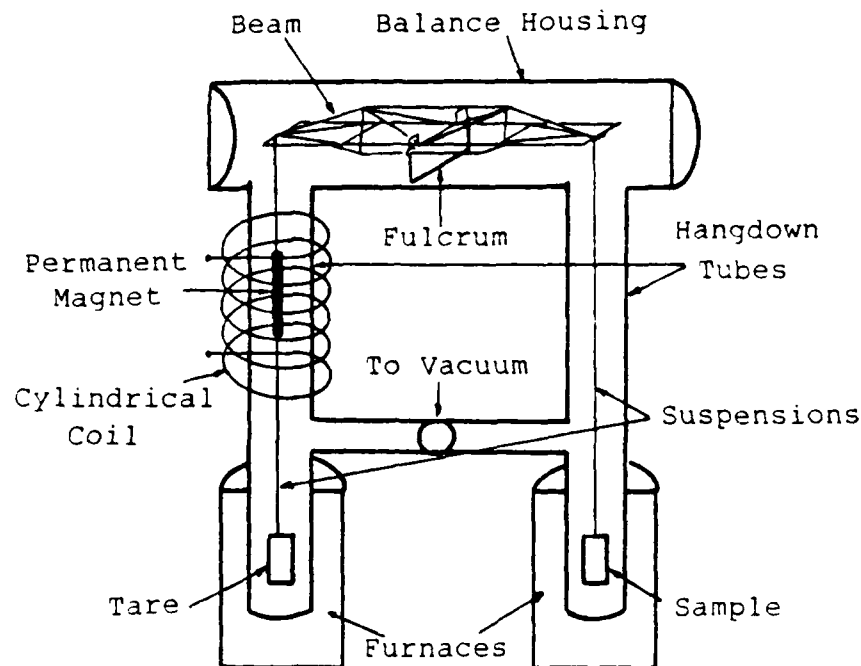


Figure II-4. Beam Microbalance of Symmetrical Design with a Trussed Beam and Magnetic Compensation. (11:29; 23:79)

other holds the counterweight and is compensated by a calibrated force, to be discussed shortly, in the system. The sensibility, or the response of the system, is on the order of a microgram, which is comparable to that of the torsion balance. The rigid parts are very rugged, and larger mass changes can be compensated with the pivotal beam balance. The system has long term stability, and the results are easily reproduced (3:1206).

Because the sample and counterweight can be held in

the same conditions to compensate for buoyancy and convection, symmetrical balances are best for sorption measurements (21:129). Adsorption studies can be tedious, so it is a great advantage to use a recorder for long term measurements with a microbalance (4:545).

#### Vacuum Microbalance Design

There are several considerations that go into the construction and use of a vacuum microbalance. Some of these considerations are; operational temperatures, outgassing properties, bake-out requirements, ultra-high vacuum considerations, and reactivity of the materials to different ambients in the system. The laboratory in which it is operated needs to be considered also. Background vibrations on the order of 20 to 50 Hz are common, and can have a serious effect on the accuracy of the balance if the vibrations have an accelerating force greater than .01 Newtons. Accelerations less than  $10^{-4}$  N will permit the operate near its maximum resolution (23:69).

Materials. The materials used in construction of a balance should be chosen such that they will not react with the test atmosphere. Quartz and tungsten microbalances are generally used (23:74), but Thomas and Williams reported the construction and use of a dural vacuum microbalance for use in argon, nitrogen, krypton and carbon dioxide ambients (27:209).

When parts of a balance are of different materials, such as a combination of quartz and tungsten, they must be bonded together. This is done with epoxy resins or metal pastes, such as silver chloride or silver platinum (23:76). Once again, these materials should be chosen so that they do not react with the ambient in such a way as to produce erroneous data.

Beam Deflection. In order to detect mass changes on the order of a microgram, a sensitive method of detecting the beam deflection must be used. Differential transformers or differential capacitors can be used to detect deflections, but they may exert forces on the balance that can cause errors in the measurement. The most widely used techniques are optical and create no undesirable forces on the microbalance. These passive detectors include: detection of angular motion of a reflected light beam, intensity changes in light that is partially cut off by a flag at the end of the balance arm, optical microscopy, or detection of optical interference patterns (23:81).

A full deflection of the beam of a microbalance was reported by Schwoebel (23:82) with a sample mass change of 0.01 %. This dramatizes the need for accurate compensation and null techniques. A null deflection and compensation force is related to the change in mass of the sample, and a calibrated force can be used as a means of determining the amount of mass gained or lost. Errors can also be avoided

that arise from the non linearity of an unbalanced beam (23:82).

Compensation. Buoyancy, electrostatic, and magnetic compensation have all been used to keep microbalances in balance. Buoyancy compensation is achieved by placing the counterweight in a chamber of a gas in which the pressure is varied and the temperature is known, and the compensating force follows Archimedes' principal (23:82). Electrostatic compensation is a method by which the force between two parallel plates is used to balance the beam in the null position (23:83).

The most widely used technique, however, is magnetic compensation. This method makes use of a ferromagnetic material sealed in a quartz tube and suspended from the balance on one side. A solenoid outside the balance housing sets up a field in the space occupied by the ferromagnetic material, thus applying a compensating force. The null is maintained by varying the current in the coil, which is proportional to the mass change of the sample (23:83).

Compensation of the beam will cause it to oscillate about the null position, so some form of damping is required to stabilize the beam at the null position. To accomplish this, the signal from the displacement detector is differentiated and amplified, and it is sent to the coil. This will automatically damp out the oscillations of



the beam, the rate of which is determined by the gain of the amplifier (23:85).

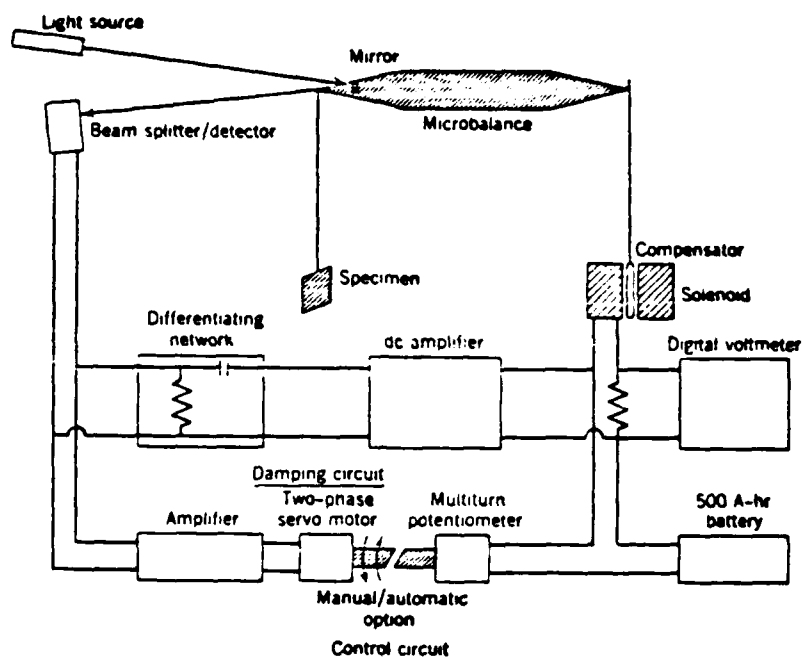


Figure II-5. Microbalance with Automatic Compensating Network. (23:85)

Figure II-5 shows the schematic of a microbalance with its compensating network. Such networks are susceptible to errors caused by power supply variations, slight solenoid position changes, and hysteresis or temperature effects of the ferromagnetic compensation weight. All of these effect the sensibility of the system(23:89).

Sensibility and Sensitivity. The sensibility of an ultragravimetric system is the response of the entire

system, including the balance and the control network, to a given upsetting force. This is the ultimate detectability of a change in mass. Sensitivity, on the other hand, is the response of the microbalance itself to an unbalancing force (23:87).

Calibration. The calibration of a balance is usually done using microweights or by the buoyancy technique. The buoyancy technique makes use of Archimedes' principal by suspending two buoyancy bulbs of equal volume and different masses in a known gas (usually nitrogen). The pressure is varied and, applying Archimedes' principal, the mass change in the sample is determined for the change in the compensation coil. This method can determine the sensibility of the instrument over wide pressure ranges (11:126). The calibration method used for this experiment is given in Appendix A.

The use of microweights is the easier and more straight forward method because there is no extra equipment needed, and it eliminates complex errors from fine measurements and calculations. This procedure involves taking a length of wire, such as tungsten, that is uniform in diameter and weighing it on an analytical balance to find it's linear density in micrograms per centimeter. Once that is found, lengths with desired masses are cut and used as microweights (23:89).

Gravimetric System. A complete system for gravi-

metric studies not only requires a sensitive microbalance, but also includes a vacuum station, a means of measuring pressure, and an adsorbate reservoir. In addition, it should have some sort of temperature control, a valve arrangement for admitting the adsorbates, and a method of recording mass changes and pressure (20:1559).

In order to keep the system clean of hydrocarbons from organic matter, such as oil from an oil diffusion pump, an ion pump or turbomolecular pump should be used. A turbomolecular pump produces vibrations that could create problems with the accuracy of the system, so a frequency damping system must be used. A Balzers 240 liters/second turbo pump was used in this study, and an isolation bellows was bolted between it and the remainder of the vacuum system to reduce the vibrations (17:242).

#### Microgravimetric Studies with Residual Gas Analysis

During the outgassing, desorption, or decomposition of a sample being studied microgravimetrically, determination of products that are being released from the sample may be of interest. A method for determining what particular vapor or gas is released is the simultaneous use of a mass spectrometer as a residual gas analyzer (RGA).

For example, when a sample is being prepared for a sorption study, one might use an outgassing, adsorption, outgassing, and reduction (OACR) cycle. This is done by

outgassing the chamber, adsorbing oxygen, outgassing the chamber once again, and chemically reducing the surface with carbon monoxide, hydrogen, or any other ambient that reacts with oxygen and is known not to adsorb on the sample (6:412). The data from the RGA will show, during the reduction step, that water is being released from the sample when it is exposed to  $H_2$  (or  $CO_2$  when exposed to CO).

Mass Spectrometers. Mass spectrometers are the instruments used to analyze the emissions of the sample during outgassing, desorption or decomposition. The instrument gives the identification and amount of a particular species present in the gas. This is done by ionizing the gas molecules present, separating the ions according to their mass to charge ratio and measuring the relative amount of a species with a given mass to charge ratio (17:234).

Ionization of molecules is usually done by electron bombardment, but is sometimes done by field ionization which produces a less complex spectra (17:234). The ionizer should be located between the sample and the vacuum pump. Furthermore, the ionizer should be in line of sight to the sample, otherwise the molecules may stick to the sides of the housing. This will complicate the analysis of the outgassed products because of complicated secondary surface relations (17:239; 28:711).

There are many ways to separate the ions, and the various RGA's are classified as: single magnetic, double focusing, multiple magnet, cycloidal, cyclotron resonance, time of flight, quadrupoles and R F, and other special analyzers (17:234). Because of its superior performance, the quadrupole RGA has virtually replaced all others. Some of the advantages are that it has no permanent magnet so it is compact and will interfere less with the balance, it is electronically adjusted rather than mechanically, it has high sensitivity at low voltages, and it is capable of rapid scanning under computer control (17:235). The quadrupole creates R F and electrostatic fields from two pairs of metal rods, in which certain species of a particular mass to charge ratio will have a stable trajectory through the filter, while other ions will be filtered out (29).

Electrical detection of the ions is done by a non-multiplying Faraday cup or an electron multiplier. The electron multiplier amplifies a single charge into a current, producing an ion current as a function of the mass to charge ratio (17:234). A schematic of an RGA is shown in Figure II-6.

RGA Measurements. The output of an RGA is a spectrum of peaks representing the atomic mass number of the species in AMU. The resolution of these peaks is given by the resolution parameter, which is the mass number divided by the width of the peak in AMU at the half maximum point.

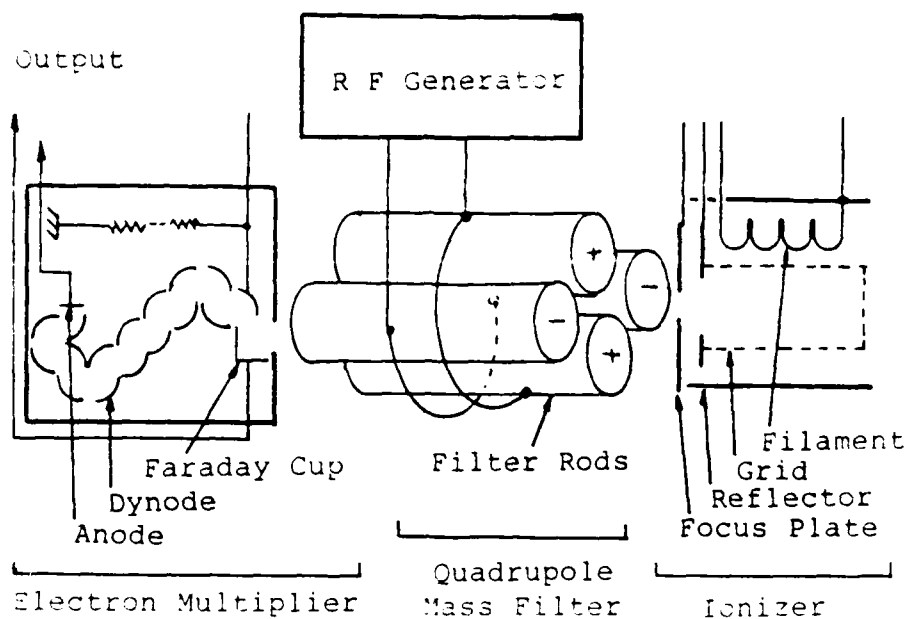


Figure II-6. Schematic of the Principal Parts of a Residual Gas Analyzer. (29)

A resolution parameter of 700 or less is good, and should allow the principal hydrocarbon (AMU 43) and  $\text{CO}_2$  (AMU 44) to be distinguishable (17:235)

Each individual gas has it's own pattern of peaks called cracking patterns. These patterns can have many peaks spread throughout the spectrum, and if more than one gas is present, peaks from several gases may occupy the same AMU, as shown in Figure II-7. With some knowledge about the gases present, the different cracking patterns can be identified (17:244). Some common peaks are; water

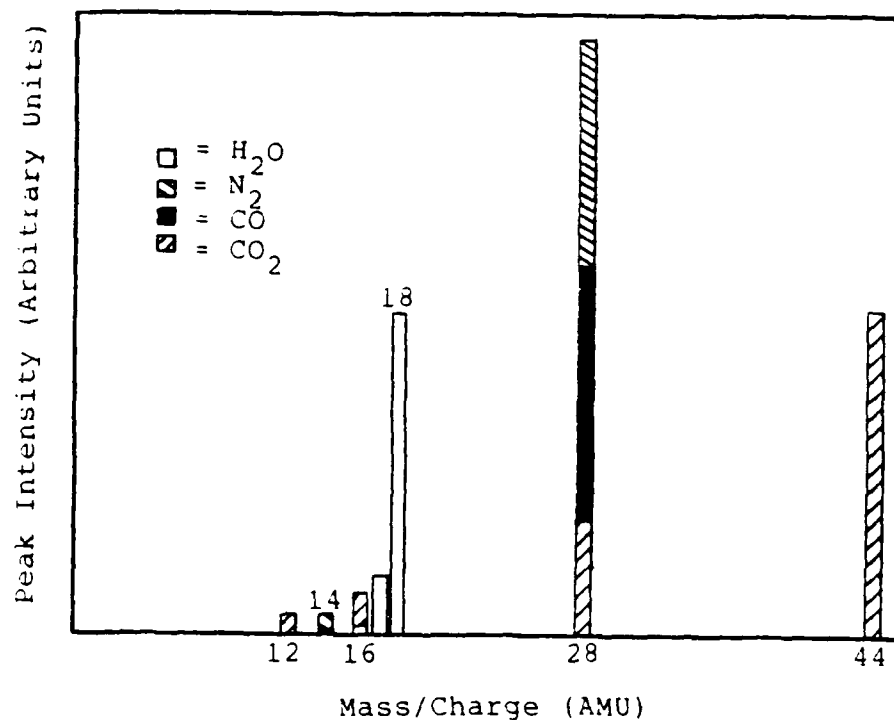


Figure II-7. Mass Spectrum of the Cracking Patterns of Four Commonly Observed Gases. (17:245)

(AMU 17 and 18), hydrogen (AMU 1 and 2), CO and/or N<sub>2</sub> (AMU 28), and CO<sub>2</sub> (AMU 44) (17:247).

Data handling is generally done on a multi-pen strip chart for recording mass change from the microbalance and the RGA spectrum. The data can be handled by a computer since RGA's are compatible (17:244).

#### Errors in Microgravimetric Analysis

When making measurements on the microgram scale,

forces that are otherwise neglected become critical to the accuracy and integrity of the data. Such forces arise from buoyancy effects, convection currents, thermomolecular flow (TMF), static electricity, and electromagnetic fields (2:272; 11:34; 21:143). TMF is most apparent in the pressure range of .01 to 1 Torr (27:220), but has been reported by Czanderna and Wolsky to occur between  $7 \times 10^{-5}$  and 2 Torr (11:38). Other spurious forces such as cavity forces and aerodynamic forces occur at greater pressures up to atmospheric pressure, while convection forces are present at higher forces (3:220). For the most part, however, of the many sources of error, corrections for TMF, buoyancy, and temperature fluctuations are needed (4:546).

Buoyancy. The buoyancy effect is the upward force exerted on the sample (or any part of the balance) by the ambient gas due to Archimedian displacement (4:546). Unless the microbalance is being used to measure the density of the gas in the system, a correction is needed for the force,  $F$ , due to buoyancy (11:37).

To understand the principal of buoyancy, the following scenario was investigated. Consider a uniform liquid of density,  $d_0$ , with an arbitrary volume,  $V_B$ , in the liquid with an arbitrary boundary,  $B$ .  $M$  is the mass of a molecule of the fluid,  $g$  is the acceleration due to gravity, and the liquid is at rest. In this situation, the total downward force is given by:



$$F_T = MV_B d_0 g - F = 0 \quad (1)$$

The buoyancy of a solid introduces some complications. The mass of the bounded volume is changed, and is not the same as the boundary of the solid. The density of the fluid remains the same outside  $V_B$ , but the density of the fluid between  $V_B$  and  $V_S$ , the boundary of the solid surface, is a function of the distance from the surface of the solid. To simplify the problem, the average density,  $d$ , is used in that volume. With  $M_S$  being the mass of the the solid, Eq (1) becomes

$$F_T = M_S g + (V_B - V_S) M d g - F \quad (2)$$

$$= M_S g + (V_B - V_S) M d g - V_B d_0 M g \quad (3)$$

or

$$F_T / g = (M_S - V_S d_0 M) + ([V_B - V_S] [d - d_0] M) \quad (4)$$

where the first term on the right side is the mass of the solid less the Archimedian buoyancy correction, and the the second term is the force due to the gas-solid interaction, which is discussed in detail by Pierotti (19:3).

The buoyancy forces discussed here are a problem that must be dealt with. The best method of compensating for these forces is to insure that the balance is symmetrical

so that equal forces will act on both sides. If that is impossible, gold wire can be suspended on the side with a net negative buoyancy, and aluminum wire of the same mass can be hung on the opposite side (21:141). Finally, the buoyancy can be calibrated and accounted for in the final form of the data.

Thermomolecular Flow (TMF). The error caused by the longitudinal flow of molecules parallel to a surface of nonhomogeneous temperature results in thermomolecular flow, giving rise to longitudinal Knudsen forces (18:100). Figure II-8 shows the effect of these Knudsen forces. TMF occurs in the pressure range of  $7 \times 10^{-5}$  to 2 Torr (11:38), and erroneous interpretation of the data may result because a large range of particle sizes will disturb isotherms over a large pressure range (27:228). Ignoring errors caused by TMF could lead to errors in evaluating thermodynamic functions such as entropy and enthalpy (27:223). Cutting and Parkyns reported an apparent mass change due to TMF of approximately 30 ug, shown in Figure II-9 (4:546).

TMF is caused by a temperature gradient in the components of the microbalance producing Knudsen forces (2:247) in the direction of hot to cold (21:149). The temperature gradient is a function of the thermal conductivity, emissivity, and coefficient of expansion in the material of the balance or sample. The error caused by TMF is directly related to emissivity and coefficient of

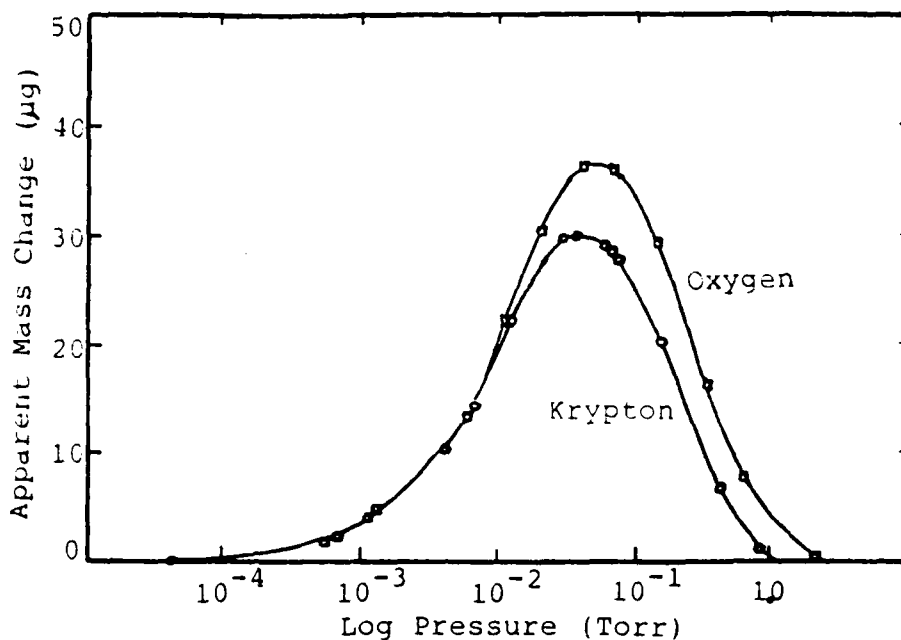


Figure II-8. Illustration of Apparent Mass Changes Caused by Thermomolecular Flow. (4:546)

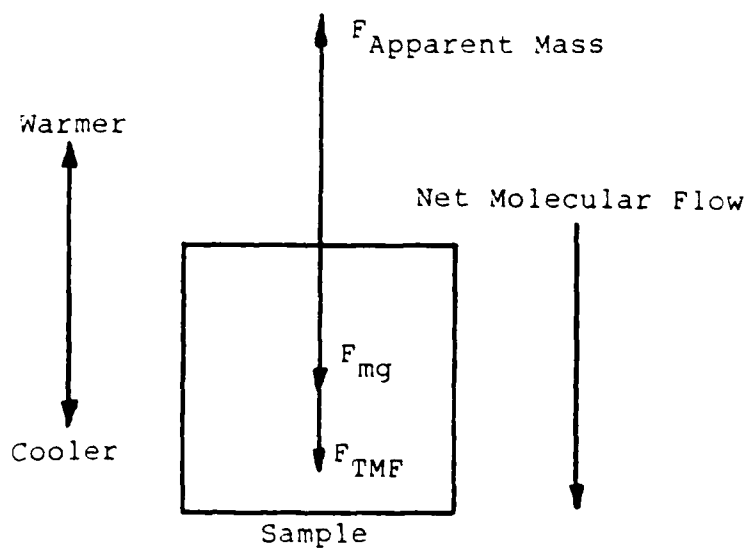


Figure II-9. Longitudinal Knudsen Forces Caused by Thermomolecular Flow.

expansion, and is inversely related to the thermal conductivity (27:211). A detailed discussion of Knudsen forces is presented by Massen and Poulis (13:100).

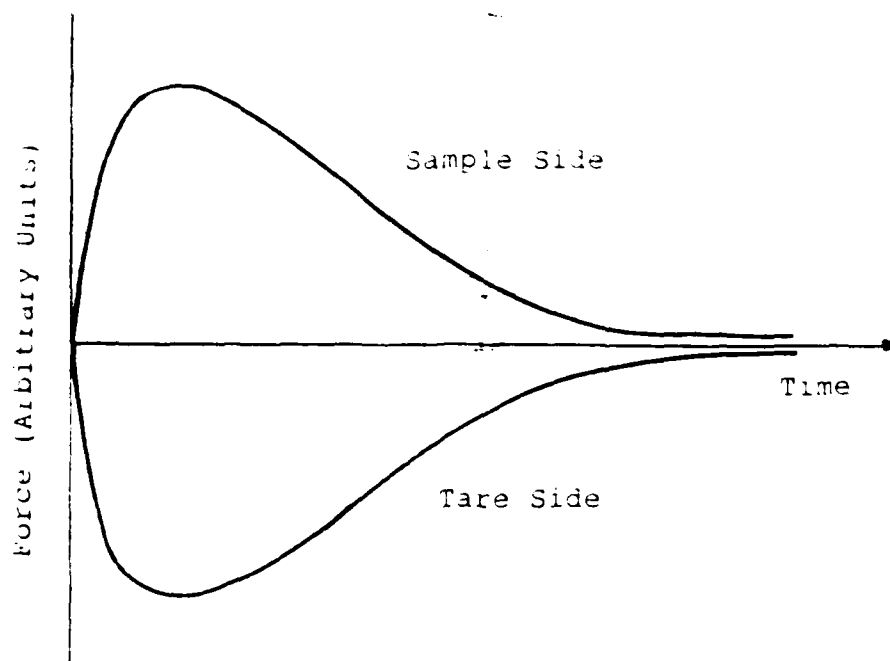


Figure II-10. Opposing Forces Acting on a Symmetrical Microbalance. (11:38)

TMF forces can be minimized by employing identical hang-down apparatuses on both sides of the balance. This includes the hang-down tubes and suspensions as well as the temperature gradient in them. This will, with an ideal arrangement, produce identical opposing forces shown in Figure II-10 (11:38). In most cases, the apparatus is not ideal, and the TMF force should be calibrated and included

in the data.

Cavity Forces. Cavity forces are related to Knudsen forces, but occur when there is a temperature difference perpendicular to the surface of a porous sample instead of a gradient parallel to the surface. The force results from a transfer of momentum between gas molecules entering and leaving the pores of the sample, and the sample itself. If the gas is warmer than the sample, the gas molecules entering the pores will have greater momentum than the molecules leaving the pores. Since the number of molecules entering the pores is equal to those leaving in equilibrium, there will be a net force in the direction towards the sample. This effect is described in detail by Massen and Poulis (18:17).

Maximum disturbances occur when the mean-free path of the gas molecules is of the order of the radius of the hang-down tubes. This is at about atmospheric pressure, which is above the pressure interval for Knudsen forces (18:17). To limit cavity forces, the pressure at which they occur can be avoided, or the temperature gradients can be eliminated or reduced to less than 1 °C per centimeter. These effects can be used to learn more about the surface geometries of the sample (18:23).

Error Compensation. Most sorption errors can be ignored because of the symmetry of the balance (11:35). However, for significant errors such as buoyancy and IMF,

the errors in the data can be corrected by using a blank of similar mass and density to the sample that does not react with the ambient (20:1564). The data acquired with the blank is related to the system, not the sample, and should be subtracted from the data taken with the sample (17:251).

### III. ADSORPTION STUDY OF MATERIALS

The adsorption study of the polyimide, gold and nickel was carried out using the ultramicrogravimetric system described below and shown in Figure III-1 (28:712). The study is broken into three sets of experiments; the polyimide study, the gold study, and the nickel study.

The goal of the polyimide study was to determine if water adsorbed on the surface of the polyimide film, and if it did, how much water adsorbed on the surface. The goal of the gold adsorption experiment was to determine if the sample adsorbed water, and if it did, determine if the water molecules could be displaced by exposing the surface to hydrogen. The aim of the nickel study was the same as the gold, with the addition of an experiment to find if hydrogen reacts with the nickel oxide on the surface of the nickel to form pure nickel and water.

#### EQUIPMENT USED

The equipment used in this study consists of an ultragravimetric microbalance with the required control system, sample changing facilities and gas handling system. A mass spectrometer is coupled to the balance and is used to monitor the gasses in the system. Other support equipment includes several gauges, an analytical balance, and a Perkin-Elmer Scanning Auger Multiprobe.

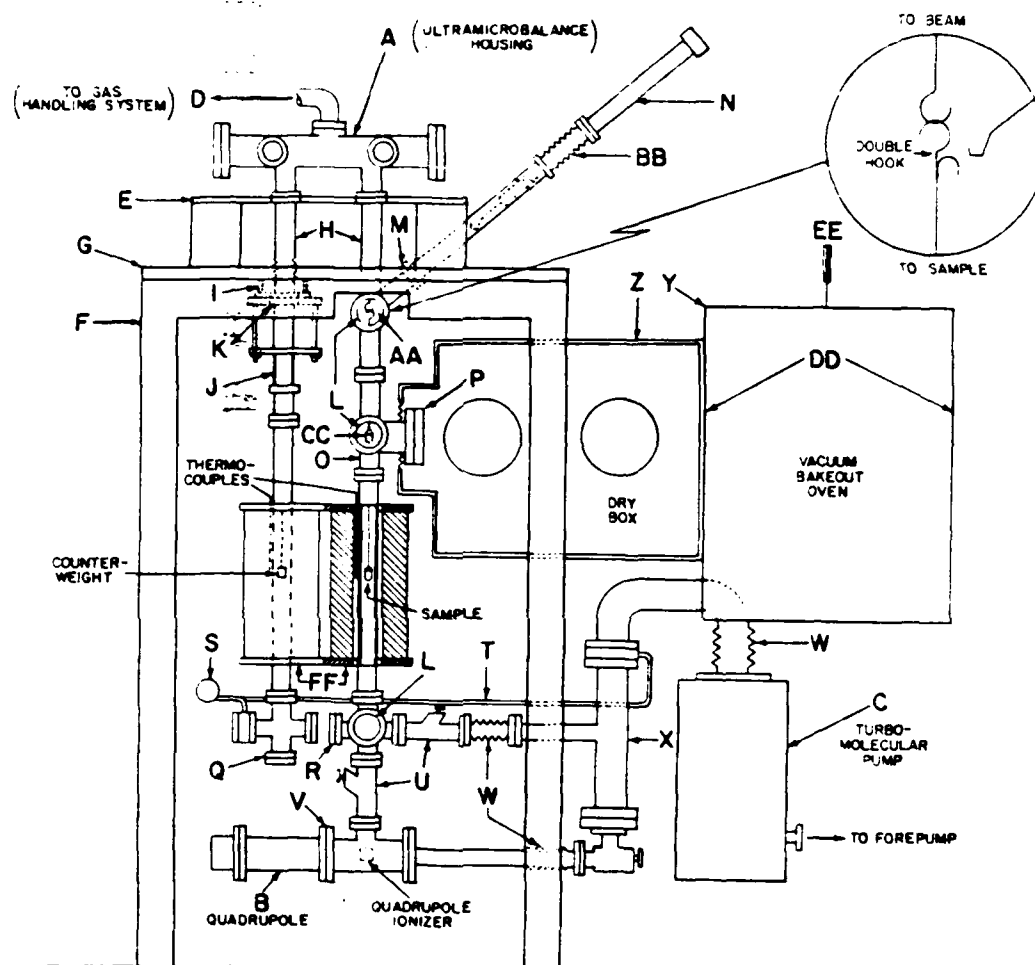


Figure III-1. Ultramicrogravimetric and Residual Gas Analyzer Apparatus for Studying Samples Loaded from a Controlled Environment. See Appendix E for Legend of Parts. (28:712)



Ultragravimetric Microbalance. The primary piece of equipment used in the adsorption study of the packaging materials was the Ultragravimetric Microbalance. The setup is shown in Figure III-1. The balance consists of a pivotal quartz beam in the form of a truss, resting on a fulcrum of tungsten points. Two quartz fibers are suspended from both sides of the beam, the right side being the sample side and the left being the tare side. A permanent magnet, encased in quartz, and a gold counterweight are also located on the tare side. The balance is enclosed by a stainless steel vacuum system with facilities for gas handling and sample changing

Control System. The control unit is an analog system which processes signal representing the deflection of the beam due to a mass change. The output is a compensating signal that returns the balance to the null position and is proportional to the change in mass.

Beam deflection is detected optically with gold flags attached to the ends of the beam. Windows in the vacuum system are located at the front and rear of the beam ends, through which infrared light is passed on one side, and its intensity is measured on the other. The system described above is shown in Figure III-2. As the beam deflects, one flag on one side of the balance drops, allowing more infrared light through, while the other flag rises and lets less light through. This deflection signal

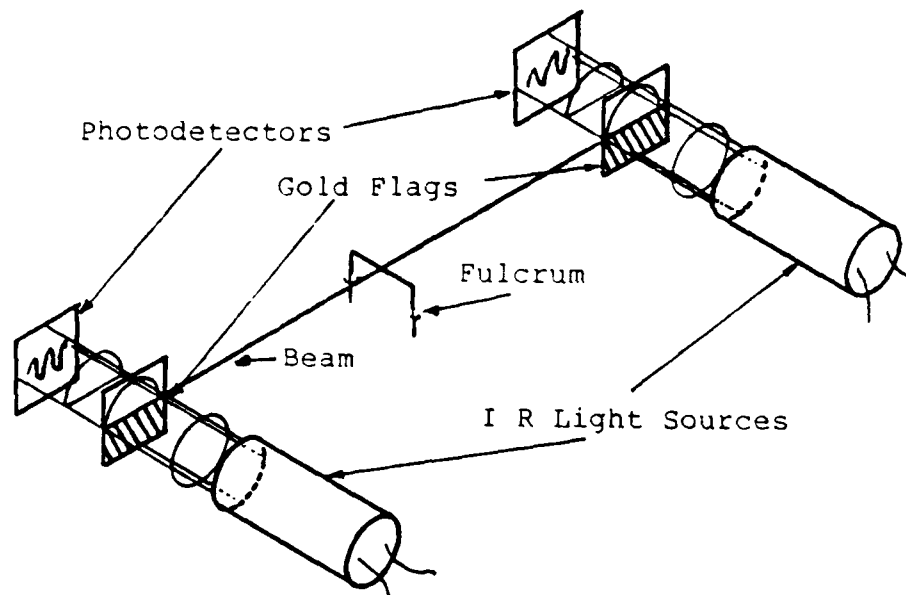


Figure III-2. Dual-path Light Sources and Photodetectors Symmetrically Located on Either Side of the Pivot.  
(9:557)

is sent to the control unit where it is processed and used to compensate the balance.

The balance is magnetically compensated by the positioning of a solenoid outside of the vacuum system, around the permanent magnet on the tare side. The compensating voltage is applied to the coil, and is related to the mass change of the sample as 1 microgram per millivolt. The calibration is presented in Appendix A.

Sample Changing. Sample changing is conducted from a plexiglass dry box that is accessed through a bakeout

oven (see Figure III-1). The dry box permits low levels of moisture of 1-5 ppm to assure a dry sample.

Sample changing is performed by detaching the sample suspension fiber from the balance, and raising the fiber so the sample is even with the access port in the dry box. With the port open, the sample can be changed from within the dry box using a Brinkman micromanipulator. With a new sample loaded, the suspension is lowered and re-attached the rest of the suspension.

Gas Handling System. The gas handling system consists of an array of four valves controlled by stepping motors to let the desired gasses into the stainless steel microbalance vacuum system. Vacuum is applied to the system initially through one such valve, using a sorption pump cooled by liquid nitrogen. When the system reaches a pressure of less than 800 millitorr, the system is opened to a turbomolecular pump, by which pressures in the  $10^{-7}$  torr range are achieved routinely.

Pressures in the system are monitored by a Granville Phillips Convection, series 275 for pressures between  $10^{-3}$  torr to 1000 torr (calibrated for  $N_2$ ), and a Granville Phillips Gauge Controller, series 270 for pressures between  $10^{-8}$  and  $12 \times 10^{-4}$  torr.

Mass Spectrometer. RGA measurements are made using a UTI 100 C mass spectrometer. The quadrupole, or mass sensor is located at the bottom of the microbalance, with

the ionizer located directly below the sample in a line of sight of both the sample and the mass filter. See Figure III-1.

Other equipment. Sample masses were measured on a Gram-atic analytical balance prior to loading them into the balance and after the tests were completed. The balance was accurate to  $0.1 \pm 0.05$  mg.

A Perkin-Elmer Scanning Auger Multiprobe, model PHI 600 was used to analyze the surface of the nickel and gold samples as well as to take scanning electron microscope (SEM) pictures of the surface.

Voltage changes across the compensating coil are sent from the microbalance controller to a Bascom-Turner recording plotter, model 8120 R. The values of the recorded points were printed by a Bascom-Turner printer, model 41013.

#### POLYIMIDE ADSORPTION EXPERIMENT

The purpose of the polyimide adsorption study was to determine if the RC-5878 polyimide adsorbed water and to determine how much water was adsorbed. The liquid polyimide was made into samples and these samples were cured in the microbalance. Each sample was exposed to increasing partial pressures of water vapor and the changes in mass were recorded.

Sample preparation. The samples were prepared by

coating a glass slide with liquid RC 5878 polyimide and pre-heating them to 100 °C to form a solid form. The films were removed from the slides, cut to size and mounted on a stainless steel sample holder. Once the mass of the sample was measured, it was loaded into the balance to be cured. Table III-1 shows the cure for each sample tested. The furnaces were calibrated by placing a thermocouple inside the hangdown tube at the sample position, and changing the settings on both furnaces. The same was done for the tare side, and the corresponding temperatures were recorded. A typical RGA spectrum for the cure is shown in Figure III-3.

RC-1. RC-1 was the thickest of the polyimide samples tested. Because the sample lost a considerable amount of mass during the cure, more mass was added to the sample side of the balance with gold wire. The system was filled with 760 torr of N<sub>2</sub> and opened to the dry box in order to add the extra gold wire tare, which was previously put in the dry box.

Once the sample was properly balanced on the beam, the microbalance was resealed, evacuated to  $3 \times 10^{-5}$  torr, and backfilled to 1 torr of nitrogen. Water vapor was added to the microbalance at 3.63 torr. After two hours, the mass was constant with a gain of 80 micrograms.

The pressure of the water vapor was increased to 5.6 torr and the sample gained an additional 140 micrograms.

Table III-1. Cure Cycles for Each Polyimide Sample Tested.

	Pre Cure 100 °C	110 °C	200 °C	400 °C
RC-1	60 min	20 min	20 min	20 min
RC-2	40 min	20 min	20 min	20 min
RC-3	35 min	20 min	20 min	20 min

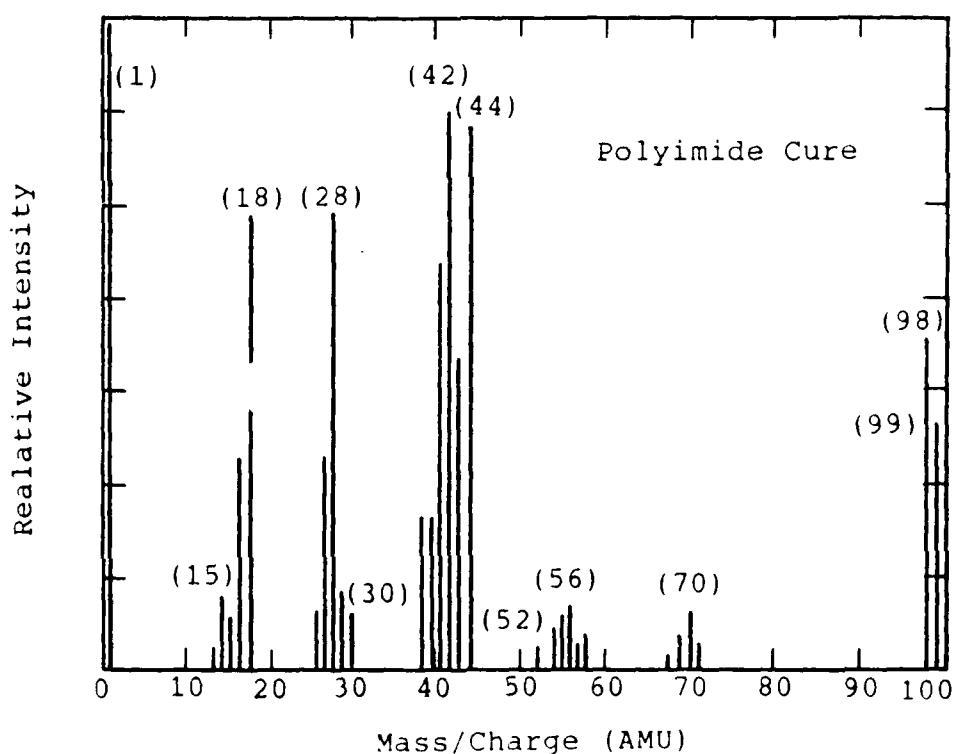


Figure III-3. Typical RGA Spectrum of the Polyimide Film During the Cure Cycle.

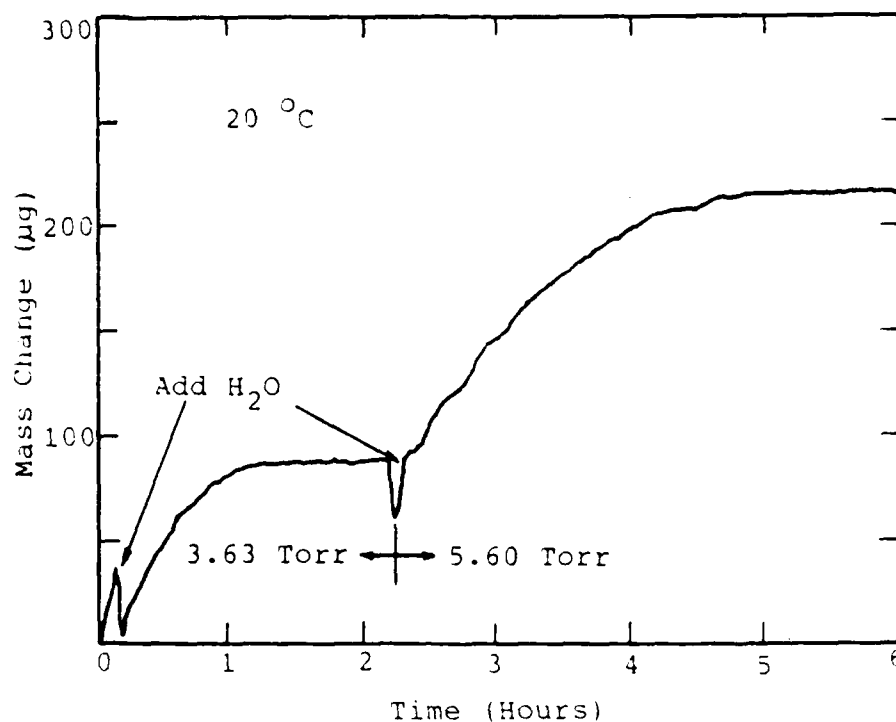


Figure III-4. Water Adsorption on Polyimide Sample RC-1.

This mass increase is shown in Figure III-4, at a temperature of 20°C. The spikes shown at the start of each rise are due to electrical pulses when valves are opened and closed and a molecular flow over the sample as the water vapor rushes in from the inlet.

RC-2. Sample RC-2 was prepared the same as for RC-1 except that RC-2 was spread on the glass slide in a very thin coat. RC-2 turned out to be the thinnest sample, but the variation in the thickness between the samples had no significance in the beginning.

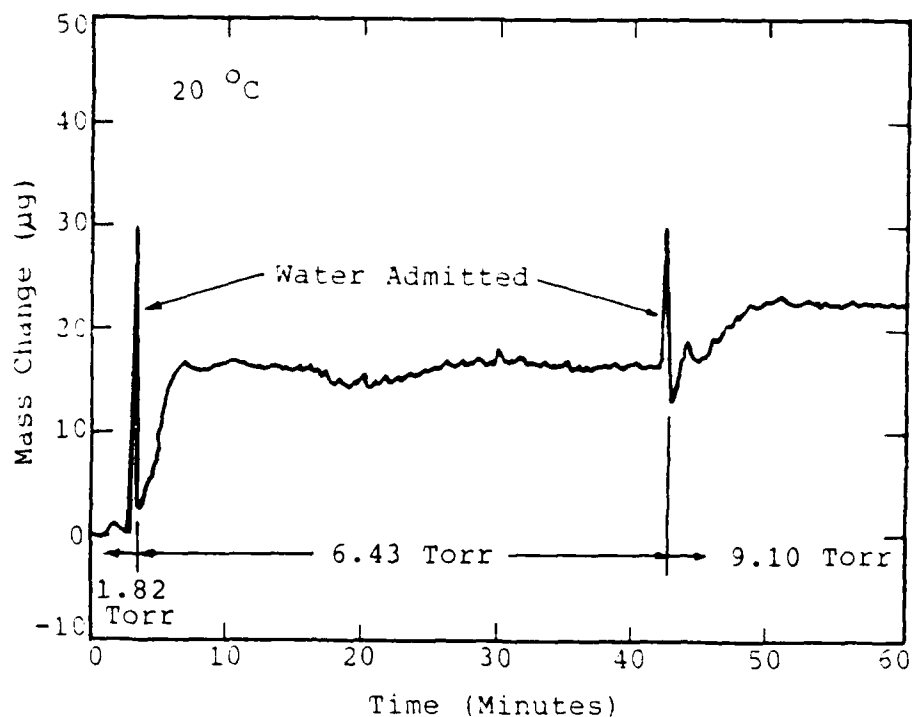


Figure III-5. Water Adsorption on Polyimide Sample RC-2.

The results of the adsorption experiment on RC-2 are shown in Figure III-5. The mass gain during the first level water vapor pressure is not shown because the balance was unstable. The remainder of the run was recorded as shown in Figure III-5 with a base pressure of 1 torr  $N_2$  and 1.82 torr of water vapor. The vapor pressure was increased to 6.43 torr and the sample exhibited a mass gain of about 16 micrograms. The pressure was increased further to 9.1 torr and the polyimide picked up 5 more micrograms before the balance became unstable again after an hour.



RC-3. RC-3 was made the same as RC-1 and RC-2, but the thickness of RC-3 was less than RC-1 and greater than RC-2. The variation in thickness between the samples was coincidental at first, but it had some significance which is discussed in the next chapter.

The sample was loaded into the microbalance and the system was evacuated to facilitate the cure. The sample was cured as before and the balance was left to cool over night. After the control system was warmed up, the background pressure of  $7 \times 10^{-7}$  torr was increased to 1

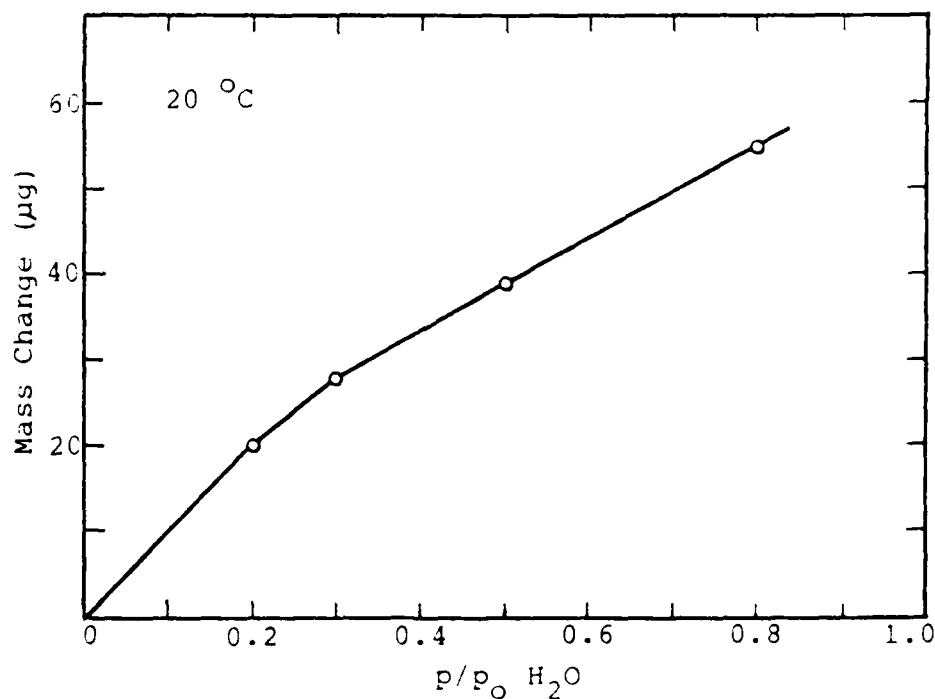


Figure III-6. Water Adsorption Isotherm on Polyimide Sample RC-3.

torr  $N_2$ . Water vapor was admitted to the system to 3.63 torr  $H_2O$ , and a mass gain of 20 micrograms was observed. The vapor pressure was increased to 5.45 torr and an additional 8 micrograms of mass was gained. An additional 11 microgram mass gain was observed at a vapor pressure of 9.33 torr, and 16 more micrograms at 14.52 torr.

These pressures correspond to partial pressures of water equal to .199 torr, .299 torr, .513 torr and .80 torr respectively. The isotherm, taken at 20°C, is shown in Figure III-6.

#### GOLD ADSORPTION STUDY

The adsorption study of the gold sample was performed to determine if gold foil adsorbes water. If the sample picked up water, the surface would have been exposed to hydrogen to find out if there is a displacement reaction between hydrogen and water on the surface of the gold, but the experiment showed no water adsorption, so the hydrogen exposure was deleted from the study.

Sample Preparation. A sample of rolled gold foil with a surface area of 100 cm<sup>2</sup> was prepared for the next experiment. The sample was rolled into a spiral as shown in Figure III-7, and held in place by 1 mil gold wire. The foil weighed 3.8537 grams, and was complemented by a gold tare weight of 2.441 grams. The total mass of gold used in this experiment was 6.2978 grams.

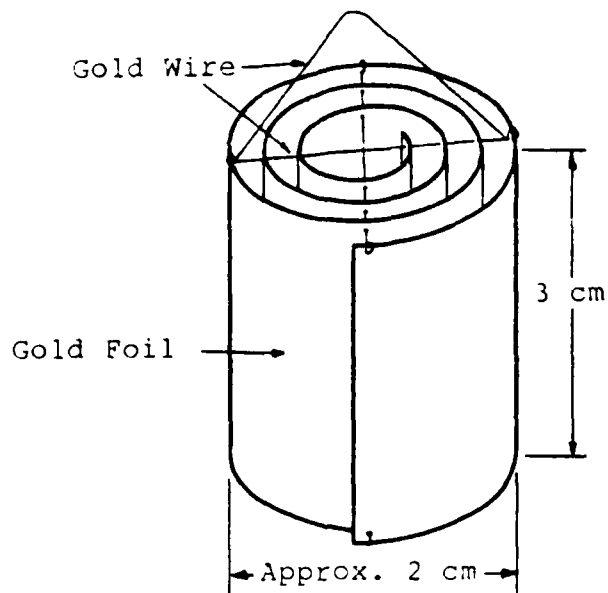


Figure III-7. Sample Configuration for Gold Adsorption Study.

The entire sample was rinsed in methanol, followed by acetone, and finally de-ionized water. It was then baked at  $200^{\circ}\text{C}$  for one hour in the bakeout oven before being loaded into the microbalance, which was heated so that the traces of residual gas in the RGA spectrum were below the RGA's noise level. The microbalance was then evacuated and re-heated to  $110^{\circ}\text{C}$  for 50 minutes. It was later realized that the rinse in methanol and acetone should have been reversed, but any residue left on the sample is assumed to have been baked off when heated.

Water Adsorption Run. The base pressure obtained in the microbalance was  $7 \times 10^{-17}$  torr before it was filled with 1 torr  $N_2$ . After warming up, the balance was zeroed and 1.87 torr of water vapor was admitted to the system. The data indicated that the sample picked up 3.5 micrograms of water. It was suspected that this data was erroneous because a sample holder that did not adsorb water exhibited a cycling mass change of the same order during a separate experiment. It was then decided that this part of the experiment be repeated.

The vapor pressure was then increased to 3.66 torr. After 40 minutes, it was noted that the balance was not properly zeroed. The controller was adjusted in real time before the microbalance became unstable, and the adjustment did not appear to upset the experiment at that time. The data showed a mass gain of 11 micrograms, but this data was not trusted, and that portion of the experiment was also repeated.

The vapor pressure was increased 5 more times to 5.45 torr, 7.28 torr, 9.09 torr, 11.41 torr, and 14.56 torr. None of these increases produced a mass change in the sample. The data is shown in Figure III-8. The system was then baked out twice in order to reduce the water peak in the RGA spectrum to the noise level to set up the next run.

The first part of the gold adsorption experiment was repeated because the first part of the previous run was

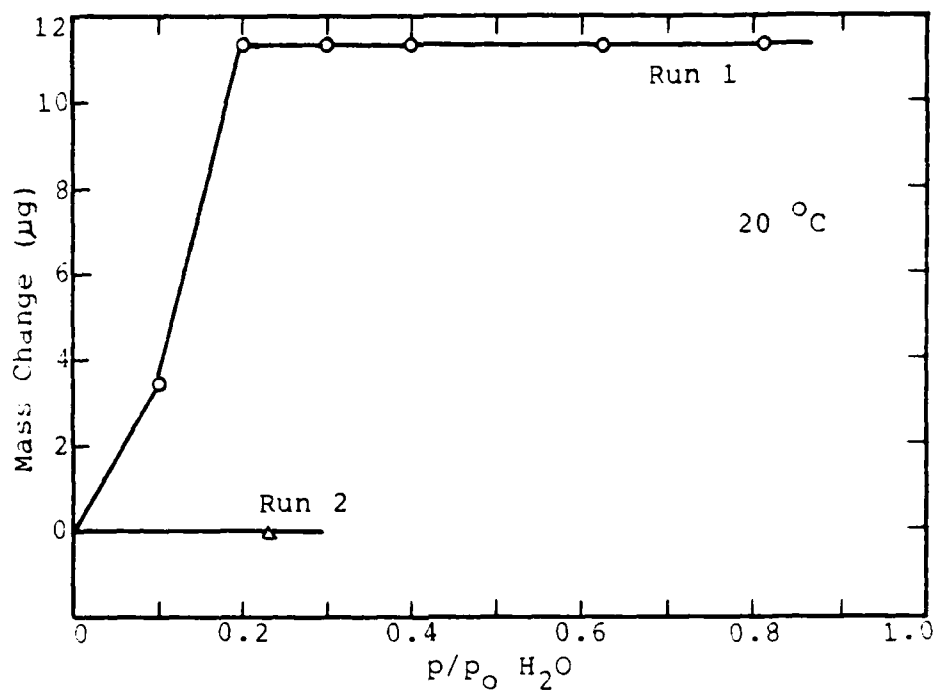


Figure III-8. Results from the Water Adsorption on Gold Foil.

probably incorrect. With a background pressure of  $7 \times 10^{-7}$  torr, the microbalance was filled with 1 torr of  $\text{N}_2$ . Water vapor was added to 4.10 torr, and there was no mass change, as expected. The microbalance was then emptied and baked out to get ready for the nickel experiment.

#### NICKEL ADSORPTION STUDY

The sample used for the nickel adsorption study was a strip of nickel foil that was prepared as explained below. The dry sample was exposed to  $\text{H}_2$  to find out if  $\text{H}_2$  reacts

with  $\text{NiO}_2$  to form Ni and  $\text{H}_2\text{O}$ . Water was then adsorbed onto the surface and a monolayer of water molecules was obtained for the last experiment. The last experiment was the exposure of  $\text{H}_2$  to the monolayer of water on the sample to determine if  $\text{H}_2$  displaces adsorbed water.

Sample Preparation. A nickel sample was prepared from a strip of nickel foil 42 cm long, 2.5 cm wide, and .025 mm thick. It was configured the same as for the gold sample, in a spiral, and was held together by gold wire. Gold wire was used because it did not adsorb water, as demonstrated by the previous experiment.

The sample weighed 2.7146 grams, and gold tare weights brought the mass up to 6.2995 grams. Before loading the sample into the microbalance, it was cleaned with a trichlorethylene rinse, followed by acetone, then methanol, and finally de-ionized water. The balance was loaded and evacuated, after which it was baked out and left to cool overnight before the next experiment.

An Auger analysis was previously performed on a piece of the same nickel foil. Figure III-9 shows a survey done after a 20 minute sputter. The survey revealed that, although the sample was very pure, there was a large amount of  $\text{O}_2$  on the surface, evident by the large peak at 516 eV. This peak is probably due to the  $\text{NiO}_2$ .

Hydrogen Exposure to Dry Nickel. The background pressure was at  $6 \times 10^{-7}$  torr when hydrogen was admitted to

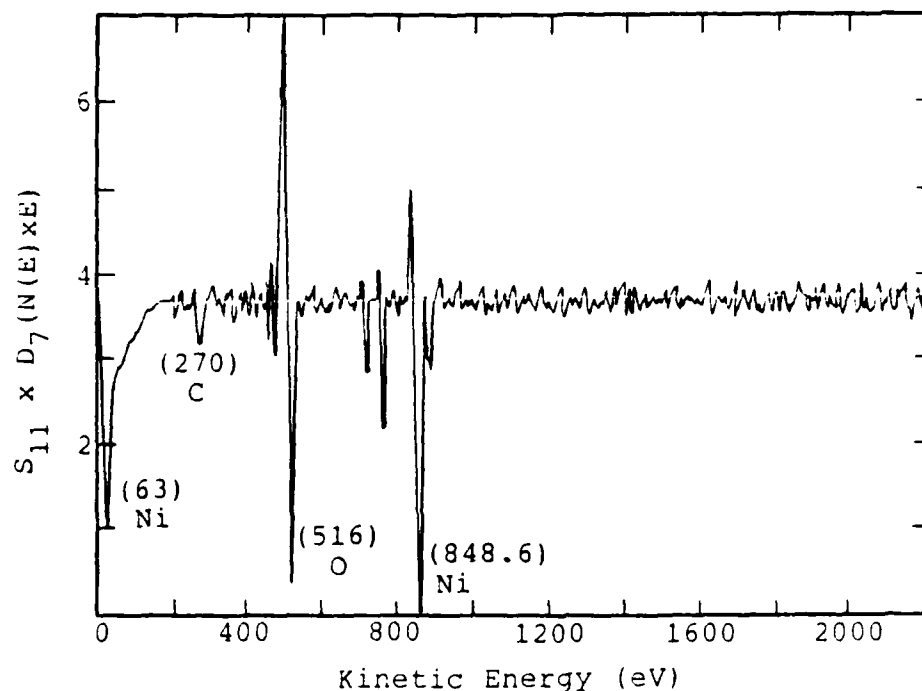


Figure III-9. Auger Analysis of Nickel Foil after Sputtering for 20 Minutes.

the system. With the system open to the turbo pump,  $H_2$  was leaked in such that the pressure remained at  $1.2 \times 10^{-5}$  torr. Initially, the output from the balance was sent to the plotter, but the output was erratic, so the balance was disconnected. The plotter was then connected to the mass spectrometer so the RGA spectra could be recorded. The first two spectra, however, were recorded by hand prior to being recorded by the plotter.

The output from the mass spectrometer showed a large peak at 28 AMU with smaller peaks at 14, 18, 32, 40 and 44

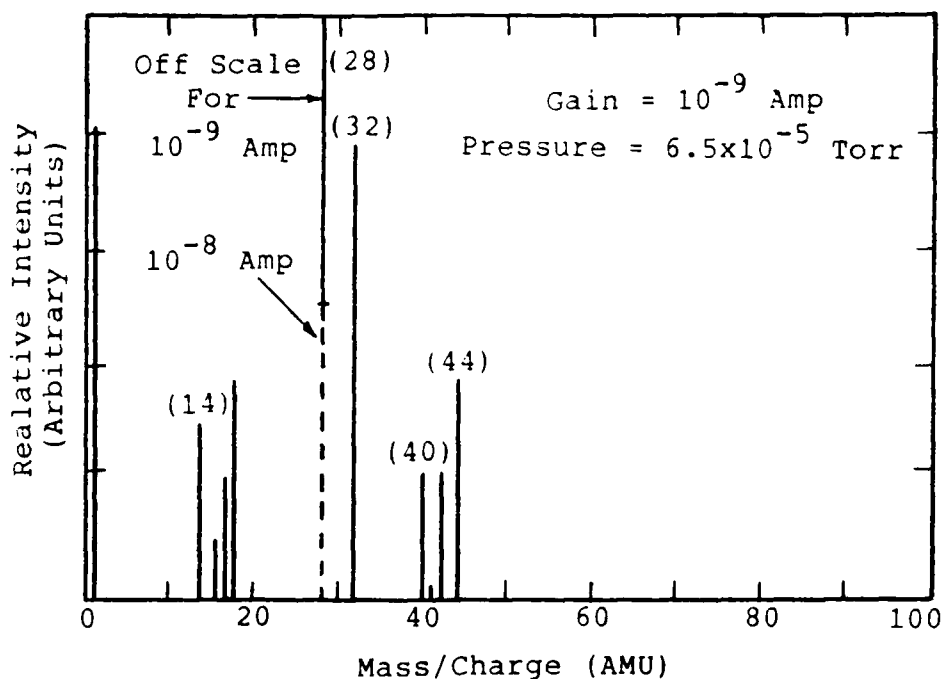


Figure III-10. RGA Spectrum of Hydrogen Exposure to Dry Nickel Sample in the Stainless Steel Microbalance.

AMU. A typical spectrum is shown in Figure III-10. The  $H_2$  rate was increased so the pressure remained at  $3.3 \times 10^{-5}$  torr, and the peaks grew in intensity but remained the same with respect to each other. The intensities decayed slowly over several minutes, as seen in Figure III-10. The pressure was increased once more to  $6.5 \times 10^{-5}$  torr, and the output reacted as before.

The  $H_2$  leak was stopped and the balance was left to pump out over night for the next experiment.

Water Adsorption on Nickel. The system was filled to 1 torr  $N_2$ , and water vapor was added to the system



while the plotter recorded the mass changes. The first step was at 0.93 torr  $\text{H}_2\text{O}$ , at which a 10 microgram mass gain was recorded when the data reached equilibrium after about four hours.

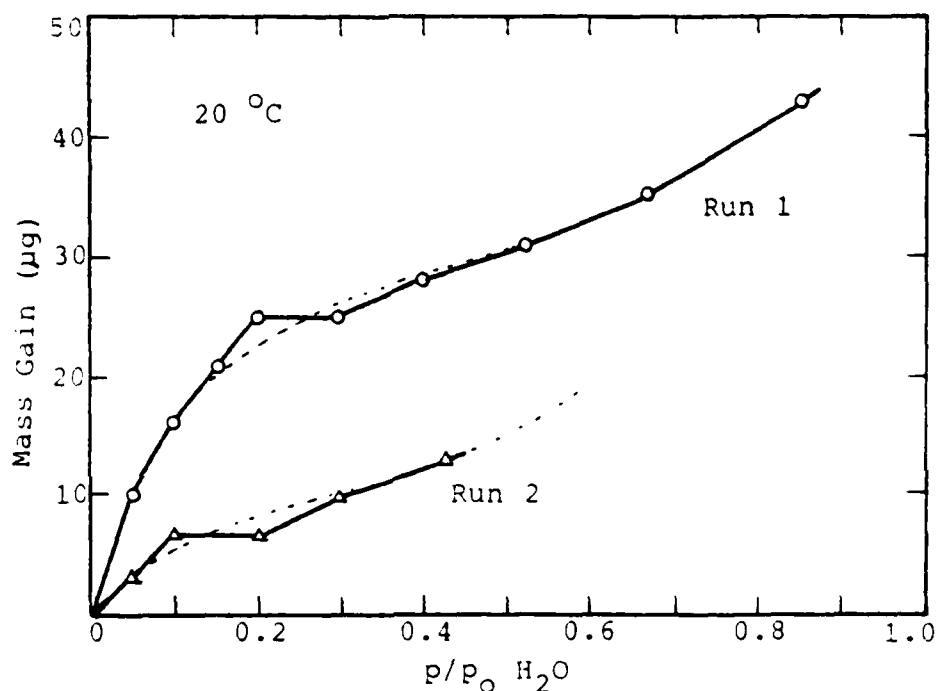


Figure III-11. Isotherm of Water Adsorption on Nickel Foil.

Several more data points were recorded, and are tabulated in Table III-2. This data was then plotted as an isotherm at  $20^\circ\text{C}$ , and is shown in Figure III-11

The system was then baked out, during which time, the sample was held at  $110^\circ\text{C}$  for 2.5 hours. The balanced cooled over night and was at  $7 \times 10^{-7}$  torr when the pump

Table III-2. Data Points Taken for the Water Adsorption on Nickel.

Pressure H <sub>2</sub> O (Torr)	Partial Pressure (p/p <sub>0</sub> )	Mass Gain (μg)	Total Mass (μg)
Run 1			
0.93	0.051	10	10
1.80	0.100	6	16
2.73	0.150	5	21
3.64	0.200	4	25
5.45	0.300	0	25
7.27	0.399	3	28
9.44	0.519	3	31
12.34	0.678	5	36
15.56	0.855	7	43
Run 2			
0.93	0.051	3	3
2.18	0.120	3	6
3.60	0.198	0	6
5.39	0.296	4	10
8.30	0.456	4	14

was closed off from the system. Without back filling the system with  $N_2$ , water vapor was admitted to 0.933 torr and the mass change was recorded. Four additional points were recorded and are tabulated in Table III-2. The isotherm is plotted in Figure III-11.

Hydrogen Effects on Wet Nickel. The system was baked out while the sample was held at  $110^\circ C$  for 6 hours and left to cool over night. The background pressure was at  $5 \times 10^{-7}$  before starting the next run.

The isotherm in Figure III-11 was analyzed using the BET surface area technique and is presented in the following chapter. The vapor pressure at which a monolayer of water molecules covers the surface was determined from the analysis to be 7.28 torr. This was the condition that was tested to determine the effects of hydrogen on adsorbed water molecules.

Water vapor was admitted to the system in two steps in order to reach 7.28 torr from a background of  $5 \times 10^{-7}$  torr. The first step was to 4.5 torr and the second step was done ten minutes later in order to let the pressure build up in the water reservoir. The balance indicated a mass increase, but it became unstable before the output reached equilibrium.

The balance was then re-zeroed and hydrogen was admitted to the system. The  $H_2$  pressure increased to 2.2 torr, and fell to 0.7 torr when the valve was closed. The

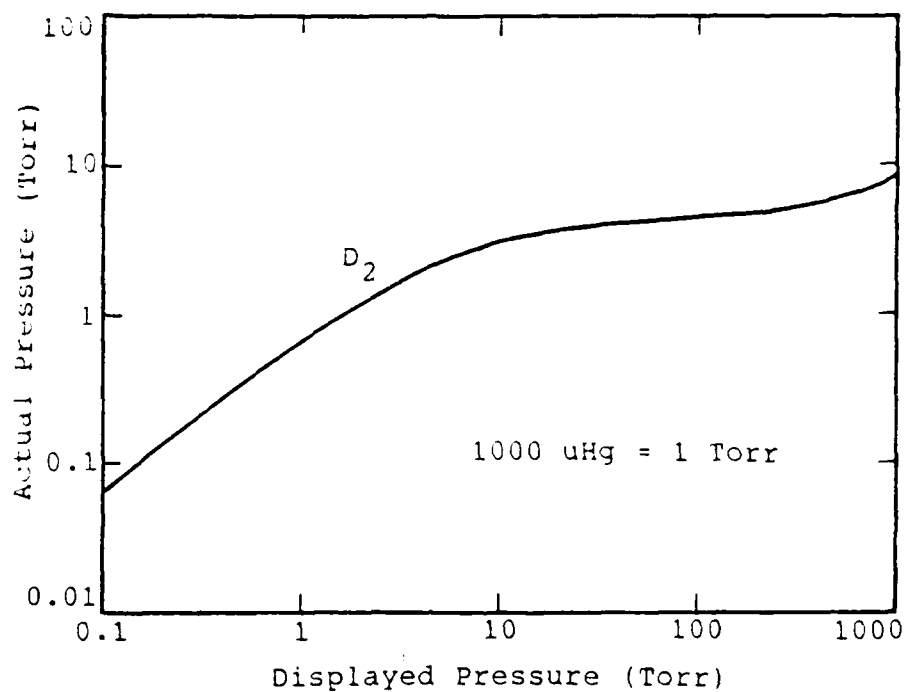


Figure III-12. Correction for Pressure Meter  
Calibrated for Nitrogen. (13:20)

Table III-3. Pressure Increases in Hydrogen with  
Corresponding Mass Changes.

Initial H <sub>2</sub> Pressure (Torr)	Final H <sub>2</sub> Pressure (Torr)	Mass Gain (μg)	Total Mass (μg)
2.2	0.7	2	2
3.3	1.0	2	4
4.0	1.4	2	6
4.2	2.0	3	9

values of the hydrogen pressures are approximations and are taken from the values of deuterium in Figure III-12. The pressure was increased three more times, and all the increases are shown in Table III-3.

Each time the hydrogen pressure was increased, the sample gained mass. The amount of mass gained was about 2 micrograms for each increase.

#### IV. RESULTS AND DISCUSSION

This chapter presents the results of the experiments performed on the polyimide, gold and nickel samples. The data from the polyimide adsorption experiment is analyzed using the BET surface area technique described in Appendix D, and discusses the relationship of the sample thickness to the amount of water adsorbed. The results of the gold adsorption study are discussed along with the significance of the data to the nickel study. Finally, the results of the nickel adsorption study are presented along with the analysis of the data and a discussion of the possible reasons for the data obtained.

##### RC-5878 Polyimide Adsorption Study

H<sub>2</sub>O Adsorption. Using the full cure suggested for the polyimide, the evidence suggests that the thickness of the polyimide film is related to the amount of water the surface will adsorb. Figure IV-1 shows the isotherm points of all three samples tested. RC-1 was the thickest sample, RC-3 was thinner, and RC-2 was the thinnest. Because of the absence of the data point for the first step in water vapor pressure is absent, the curve of RC-2 was adjusted for the worst case condition. This case exists when the mass gain at the first step in pressure for RC-2 is equal to the mass gain of RC-3 at the same pressure. Several

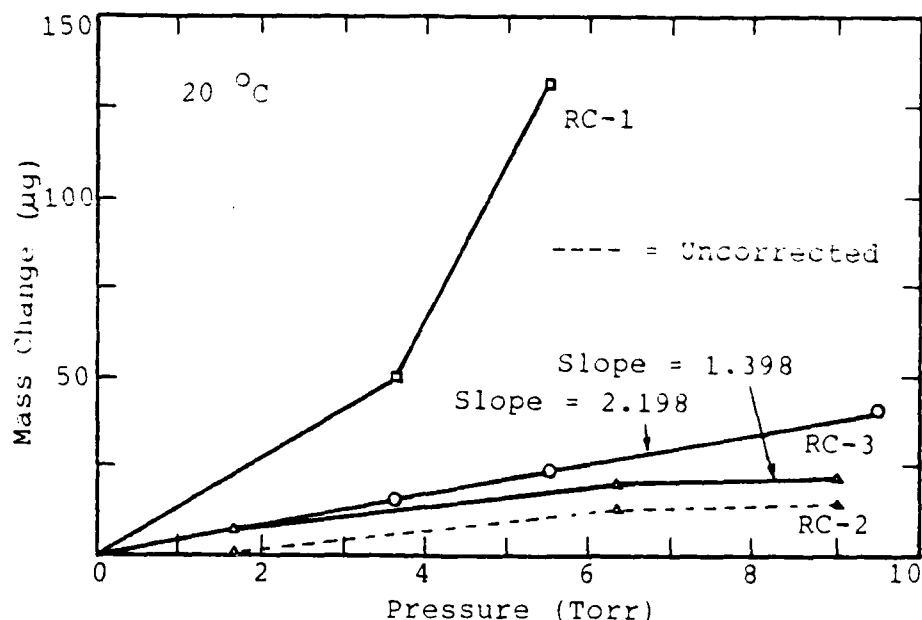


Figure IV-1. Isotherms of Water Adsorption on RC-5878 Polyimide Samples RC-1, RC-2 and RC-3, Normalized to 100 square centimeters Surface Area.

reasons are given for this assumption.

This assumption was arrived at for several reasons. First, the mass gains are presented as relative values for samples of normalized surface area as measured, and since RC-1 gained much more mass than RC-3, the assumption was made that RC-2 would not gain more than RC-3. Second, the rate of mass gain between 6.43 and 9.1 torr of RC-3 is 2.198 micrograms per torr  $H_2O$ , which is greater than that of RC-2 at 1.398 micrograms per torr (both normalized to 100 mm<sup>2</sup> surface area).

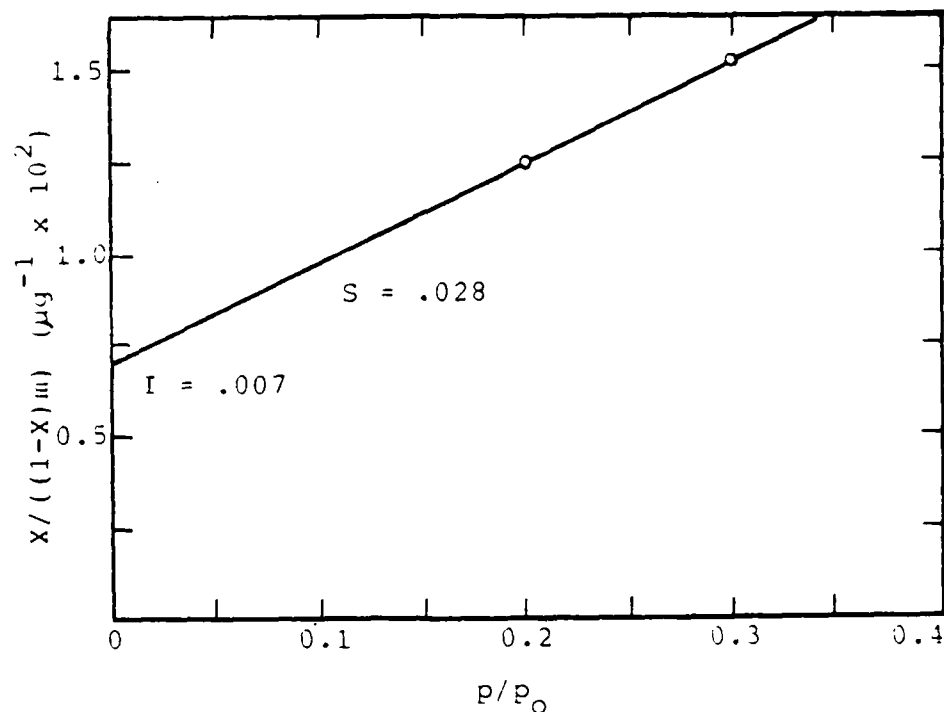


Figure IV-2 BET Plot of RC-3 Adsorption Isotherm for BET Surface Area Analysis.

BET Surface Measurement. The adsorption isotherm for RC-3 was analyzed using the BET surface area technique. This technique is explained in Appendix D (5:194; 21:159). The isotherm was replotted as  $X/((1-X)m)$  for the pressures between 0.91 and 6.37 torr, where  $X$  is the partial pressure of  $H_2O$  at  $20^\circ C$ , and  $m$  is the mass gained in micrograms. The plot is shown in Figure IV-2.

The slope of the line in Figure IV-2 is  $S = 0.028$  and the intercept is  $I = 0.007$ . Using these values, the mass for a monolayer coverage of water,  $m_m$ , is



$$m_m = 1/(S+I) = 28.57 \mu g \quad (1)$$

Using the value of  $W_g = A_m N_A / M = 4180 \text{ m}^2/\text{g}$  from Robens (21:157), the calculated surface area of RC-3 is

$$A_s = m_m W_g / 1000 = 1.194 \text{ cm}^2 \quad (2)$$

which is only 7.8% less than the measured area of  $1.295 \text{ cm}^2$ .

#### Gold Adsorption Study

The water adsorption experiment on the gold surface showed that there was no mass gain when a sample of rolled gold foil was exposed to an ambient of water vapor. This does not necessarily mean that no gold will adsorb water, only that rolled gold foil does not adsorb water at  $20^\circ\text{C}$ . This does, however, mean that the gold used in this experiment can be used as a tare weight for other adsorption experiments without affecting the data.

#### Nickel Adsorption Study

Hydrogen Exposure to Dry Nickel. The exposure of hydrogen to the dry nickel surface resulted in a large peak at 28 AMU on the RGA spectrum, which indicates nitrogen or carbon monoxide. Other peaks present, in decreasing

intensities, were 32 ( $O_2$ ), 44 ( $CO_2$ ), 18 ( $H_2O$ ) and 14 (N) AMU.

An Auger scan of the nickel foil before sputtering is shown in Figure IV-3. This shows that the nickel had a considerable amount of carbon as well as oxygen on the surface. The  $O_2$  is due to a strong oxide ( $NiO_2$ ), and the carbon was probably from the plastic package the sample was stored in, or the solvents used to clean it .

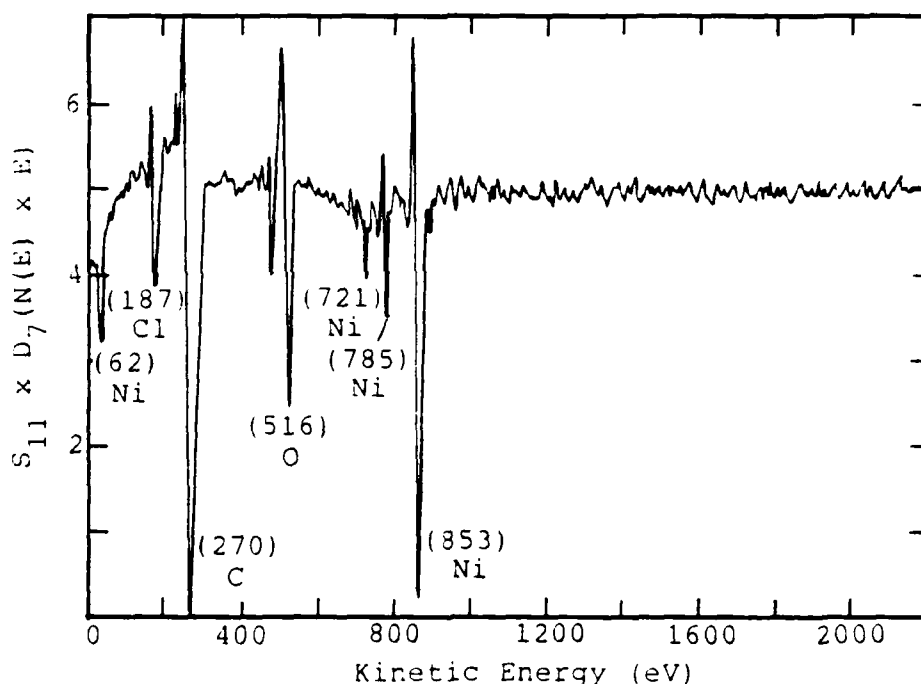


Figure IV-3. Auger Scan of Nickel Foil Before Sputtering.

When the system was flooded with hydrogen, the resulting peak at 28 AMU might have been from the  $H_2$

molecules displacing CO, but that was unlikely because the oxygen would tend to react with the CO to form CO<sub>2</sub>. This means that the peak at 28 AMU was nitrogen. Since the Auger scan did not show any N<sub>2</sub> on the nickel, it must have come from a displacement reaction on the walls of the balance housing. Since any of the molecules shown in the RGA spectrum could have been on the walls of the balance, the RGA data from these tests cannot be used to determine if a displacement reaction or oxide reduction occurred on the nickel surface.

Water Adsorption on the Nickel Surface. The first water adsorption experiment on the nickel resulted in the adsorption isotherm shown in Figure IV-4. The shape of the isotherm is a classical type II, or BET isotherm, which was analyzed using the BET surface area technique. The data points between 0.91 and 6.37 torr were replotted as  $X/((1-X)m)$ , and the new plot is shown in Figure IV-5.

The slope and intercept of the line are 0.04650 and 0.002111 respectively. Inserting these numbers into equation (1), the mass for monolayer coverage,  $m_m$ , becomes 20.57 ug. Using  $W_g = 4180$  as before and applying equation (2), the surface area was 0.860 cm<sup>2</sup>. This result is surprisingly low, since the measured surface area was 210 cm<sup>2</sup>.

The data from the Auger analysis explains why the surface area from the BET analysis was so small. Since

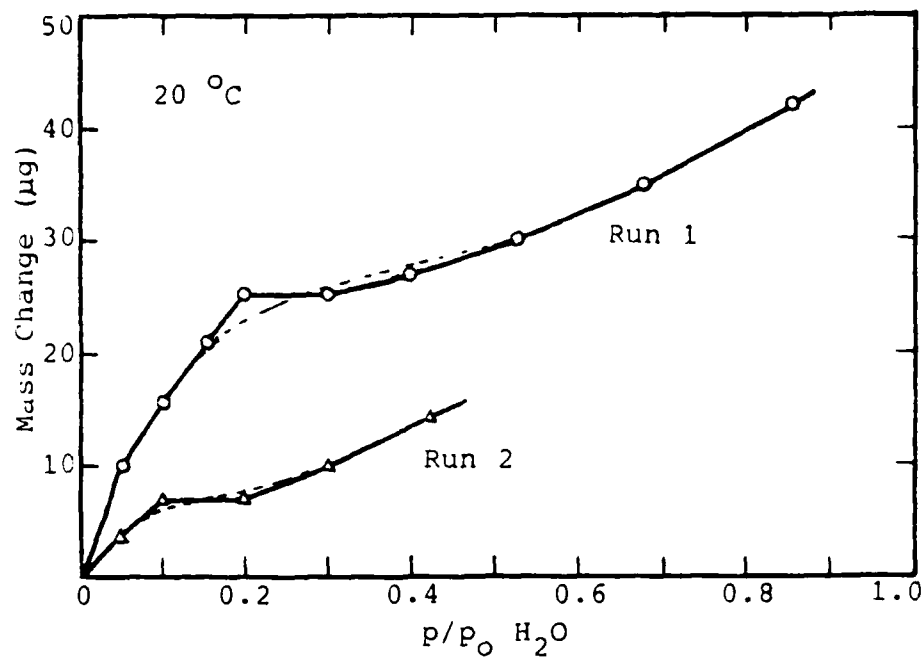


Figure IV-4. Isotherms of Water Adsorption on Nickel Foil.

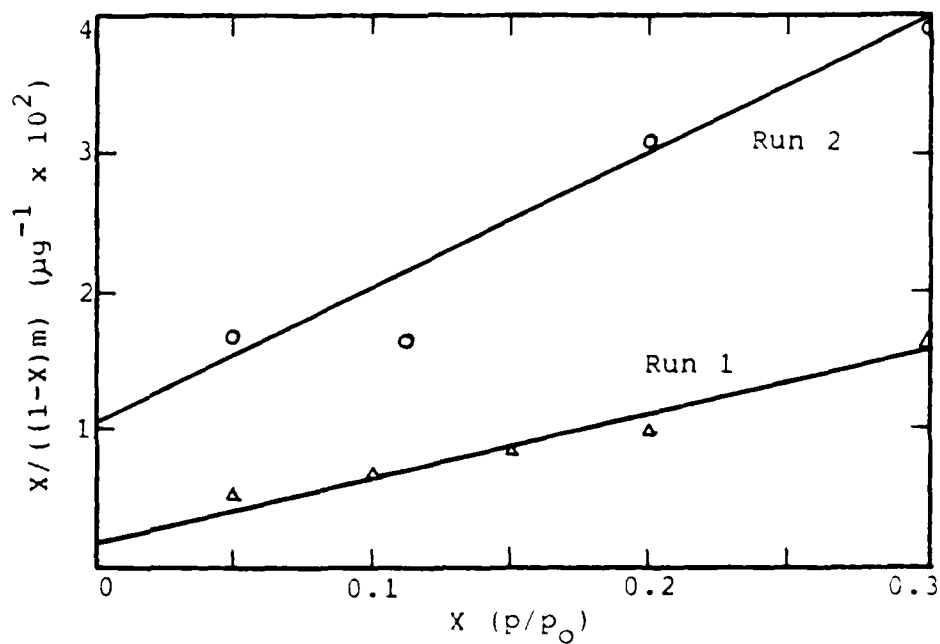


Figure IV-5. BET Plots of Figure IV-4 for BET Surface Area Analysis.

the BET analysis only shows the active adsorbing surface, the rest of the surface must have been passivated by the nickel oxide that was so predominant in the Auger scan.

A second adsorption experiment was performed on the sample without a background of 1 torr  $N_2$ , but since nitrogen is inert to the reactions taking place, the change had no effect on the data (1:66). The isotherm, also shown in Figure IV-4, shows less mass gain than before and is not as smooth. With the curve smoothed out to a classical BET isotherm and replotted as shown in Figure IV-5, the surface area was calculated to be  $0.3958 \text{ cm}^2$ .

This 54% reduction in surface area probably means that more nickel oxide was grown and passivated the surface even further. Some of the nickel atoms from the active surface area could have reacted with the oxygen atoms from the water molecules, forming  $NiO_2$ .

Hydrogen Exposure to Wet Nickel. The active area of the nickel sample was covered with a monolayer of water molecules and exposed to hydrogen. The expected results were that the sample would lose mass as the hydrogen atoms displaced the water molecules adsorbed on the surface. The results of the experiment, however, showed a mass gain with each increase in hydrogen pressure, as seen in Figure IV-6.

The increases were not instantaneous, so they were not caused by buoyancy effects. Instead, the mass gains can be

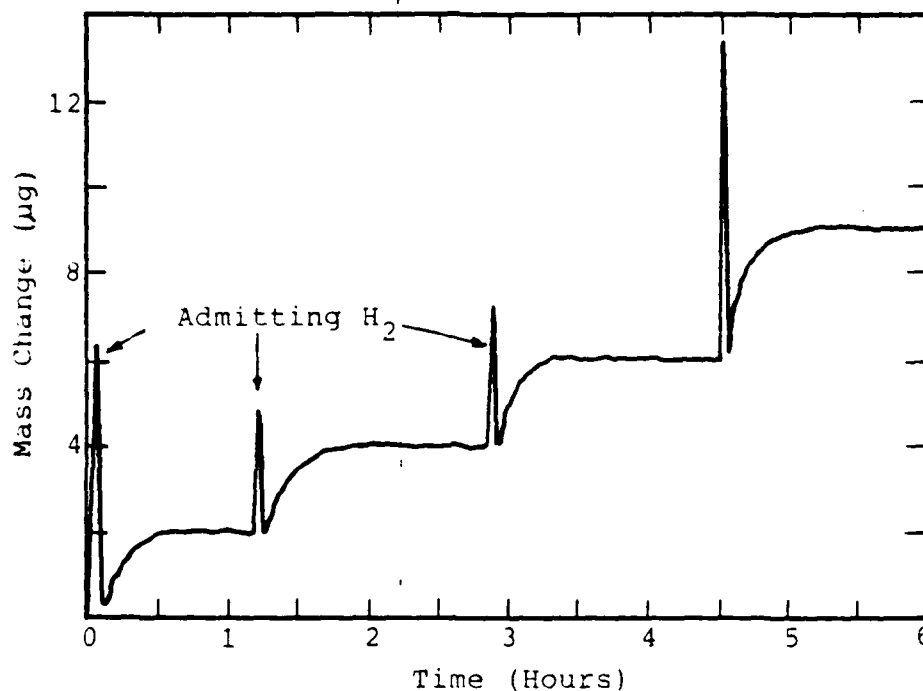


Figure IV-6. Hydrogen Exposure to Nickel Surface with Monolayer Water Molecule Coverage.

explained by the phenomenon of hydrogen bonding. In hydrogen bonding, the hydrogen atom tends to appear as a bare proton because its electron is being devoted to the bond between the two hydrogen atoms. This means it is attracted to small electronegative atoms such as the oxygen atoms in the  $\text{NiO}_2$  (24:378). Since the area of  $\text{NiO}_2$  was so much greater than that of the active nickel surface, the net mass change was a gain, even if there was a displacement reaction taking place.

## V. CONCLUSIONS AND RECOMMENDATIONS

This section discusses the conclusions drawn from the results presented in the previous chapter. Some practical applications of the findings are also given along with some recommendations for further study.

### Inferences from the Results

Polyimide Film. The results show that the RC-5878 polyimide adsorbs water vapor at room temperature, and the thickness of the film is directly related to the amount adsorbed. This means that the amount of water that is adsorbed by the film may be controlled by the thickness, and might result in less water being released into an integrated circuit package.

Gold Foil. The results showed that the rolled gold foil did not adsorb water vapor at room temperature. This means that gold foil can be used successfully in integrated circuit packages without running the risk that it could introduce water vapor into the package when the circuit operates at elevated temperatures. Swartz, et al. (25:52) and Thomas and Sharma (25:549) found that evaporated gold did adsorb water vapor that could be released into the integrated circuit package during operation. If the lids in the study done by Swartz, et al. (25:52) were replaced with gold foil, for instance, there would be no adsorbed

water to vaporize inside the package.

Nickel Foil. The results of the nickel adsorption study show that there was only a small portion of the total area that adsorbed water because most of the nickel was passivated by nickel oxide, which did not adsorb water. Also, the observation was made that more of the surface was passivated after the sample was exposed to water vapor. These observations suggest that nickel used in integrated circuit packages is safe from the standpoint of contamination from water vapor, as long as the entire surface is passivated with nickel oxide. This would rule out using deposited nickel, unless it was allowed to oxidize before being sealed in a package.

#### Recommendations for Further Study

TAB Film Adsorption Study. To learn about the adsorption properties of materials actually used in integrated circuit packages, the actual components should be studied. In the case of polyimide films, adsorption studies should be performed on film that is produced for tape automated bonding (TAB).

The tests that are recommended for a polyimide TAB film include plotting adsorption isotherms at room temperature and at operating temperatures to observe the adsorption properties in those environments. Also, desorption tests could be performed to determine how much



water vapor, if any, would be released into the integrated circuit package at elevated temperatures.

Sputtered Gold Adsorption Study. Sputtered gold, as opposed to gold foil, is used in the package on the lids, and has a different texture than the foil. This different texture might allow for water adsorption, so its adsorption properties should be studied in order to support or deny this claim.

The same tests described for the polyimide TAB film should be performed on the sputtered gold, unless early experiments show that, like gold foil, sputtered gold does not adsorb water.

Further Nickel Studies. The first experiment recommended for further study on the nickel is to perform the same studies presented above for the polyimide and the gold, except they should be performed on a pure unoxidized nickel sample surface. By reducing the nickel oxide on a pure sample, the adsorption properties of the nickel, without having to account for reactions that may be taking place on the oxide, can be studied more accurately. Oxide reduction can be accomplished using an OAOR cycle explained in Chapter II.

The second suggested experiment involves plotting hydrogen adsorption isotherms for both a reduced nickel surface and a totally oxidized surface. These tests would verify or deny the existence of hydrogen bonding on the

nickel oxide, as was used to explain the mass gain observed when the wet nickel sample was exposed to hydrogen. Hydrogen bonding would be supported if hydrogen exposed to the  $\text{NiO}_2$  gained mass, while a pure surface exhibited no mass gain.

The final nickel study proposed would involve continuation of the experiments described above. After exposing water vapor to a pure, unoxidized nickel surface, hydrogen could be admitted to the system to determine whether the hydrogen displaces the water molecules adsorbed on the surface, characterized by a loss in mass. Without the  $\text{NiO}_2$  on the surface, hydrogen bonding would not be a factor.

Microbalance Computer Control. The final recommendation for further study is to build and test the personal computer controller suggested in Appendix C. By converting the analog error signal from the beam deflection detectors to a digital signal, it can be sent to a personal computer to be processed. The output can then be converted back into an analog signal that will apply a compensating voltage to the restoring coil on the balance. This controller will provide easier access to data taken by the microbalance.

This computer control will provide an opportunity to expand the entire system to computer control. This may include control of gas handling systems, temperature

control, and decision making such as when an adsorption has reached equilibrium.

Considerable work was done on such a controller, and one was actually constructed, but the sensibility of the new system was 50 micrograms per millivolt, as opposed to the current sensibility of 1 microgram per millivolt (12). This system is presented in Appendix C, along with the modified version.

## APPENDIX A: MICROBALANCE CALIBRATION

The calibration of the microbalance was performed using the buoyancy technique described by Czanderna and Honig (6:1208). This was accomplished using a sealed buoyancy bulb and a tantalum weight of equal masses and different volumes. The bulb was loaded into the balance and nitrogen was admitted at a series of pressures. As the pressure changed, so did the force acting on the buoyancy bulb due to Archimedes' principle. The change in force caused the balance to deflect, which was compensated by a change in voltage across the restoring coil. The data was recorded and is tabulated in Table A-1 and plotted in Figure A-1.

Table A-1. Calibration Using the Buoyancy Bulb.

Run 1			Run 2		
P (Torr)	dV (mV)	V (mV)	P (Torr)	dV (mV)	V (mV)
700	0	0	820	0	0
600	.479	.479	700	.594	.594
500	.492	.971	600	.444	1.038
200	1.190	2.161	500	.432	1.470
100	.524	2.685	400	.508	1.978
1.3	.559	3.244	200	.926	2.904
			100	.473	3.377
			1	.549	3.926

Table A-2. Calibration Run Using the Tantalum weight.

Run 1				Run 2	
P (Torr)	V (mV)	P (Torr)	V (mV)	P (Torr)	V (mV)
700	91.1	100	72.7	1	66.4
600	87.8	200	75.6	100	70.0
500	85.0	300	78.3	200	72.9
400	82.2	400	80.9	300	75.4
300	79.5	500	83.7	400	78.2
200	76.6	600	86.9	500	80.0
100	74.4	700	90.1	600	84.4
1	70.9			700	86.7

The buoyancy bulb was replaced by the tantalum weight and a second calibration run was performed. The data is shown in Table A-2, and the graph of compensating voltage v.s. pressure of nitrogen is shown in Figure A-2. By using the difference between these two slopes, the sensibility of the balance is

$$S = M(V_1 - V_2)10^6 / (S_1 - S_2)ZPV \quad (1)$$

where

$S$  = balance sensitivity ( $\mu\text{g}/\text{mV}$ )  
 $M$  = molecular weight of nitrogen (28.016 g/mole)  
 $V_1$  = buoyancy bulb volume ( $3.375 \text{ cm}^3$ )  
 $V_2$  = tantalum weight volume ( $0.0278 \text{ cm}^3$ )  
 $S_1$  = slope obtained using the buoyancy bulb  
 (-4.6173 mV/Torr)  
 $S_2$  = slope obtained with the tantalum weight  
 (0.02821 mV/Torr)  
 $P$  = pressure at 1 ATM  
 $Z$  = correction for the nonideality of nitrogen  
 (1.0915)

$10^5$  = conversion factor ( $10^5 \mu\text{g/g}$ )

Using the relation above, the sensibility of the microbalance is 1.086 micrograms per millivolt.

It should be noted that, because of time constraints, the actual calibration runs were carried out by laboratory personnel at an earlier date. The recorded data was used to arrive at the sensibility described above.

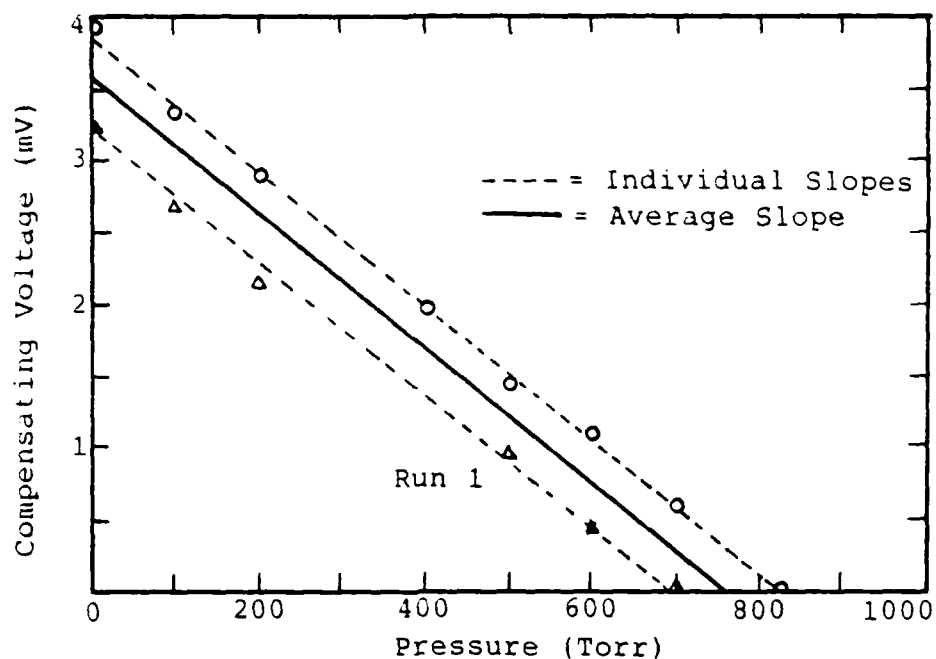


Figure A-1. Calibration Curve for Buoyancy Bulb in Nitrogen.

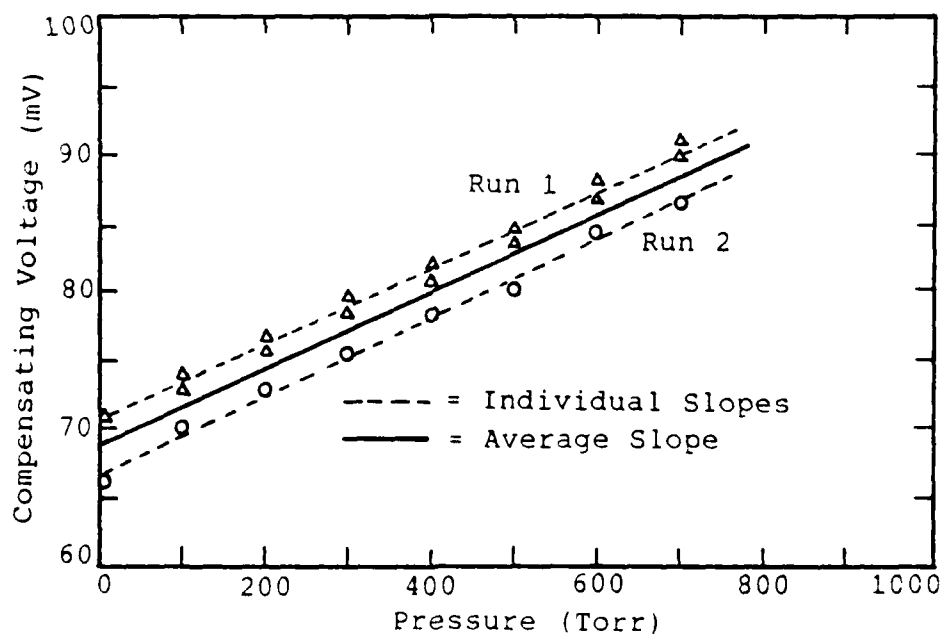


Figure A-2. Calibration Curve for Tantalum Weight in Nitrogen.

## APPENDIX B: MICROBALANCE OPERATION

The heart of the microbalance control system is the analog control circuit shown in Figure B-1. A signal representing the beam deflection enters the controller through A1 (all operational amplifiers are FMI OP-07) and splits into two paths. The top path leads to A2, a derivative compensator circuit, which produces a signal that is out-of-phase with the restoring signal, which is discussed below. This out-of-phase signal limits the response of the restoring signal in order to prevent mechanical damage to the balance.

When the balance is operating properly in the null position, the current from the differentiator is zero, as shown on the zero meter. During start-up, zeroing is accomplished by adjusting the tare switch, which electronically varies the the effect of the counterweight by sending a rough compensating signal to the coil. This signal brings the balance to within the range of the compensating network which brings the balance to the null position.

The lower path leads to the circuitry which produces the restoring signal. The deflection signal is filtered through a low pass filter to eliminate any high frequency noise and pass the signal that is on the order of 1 Hz. The signal is then buffered at A3 and sent to A4, where it



is amplified and clipped to produce a signal that resembles a square wave. When the balance is in the null position, this signal is actually a square wave, and the null meter flips back and forth, spending equal time on each side. If the balance falls off of the null position, the null meter spends more time on one side than the other, and eventually stays pinned on one side.

The square signal is sent to a zeroing circuit where it is used both as a floating ground for the power supply, and as an input to the rest of the circuit. A voltage divider between the power supply voltage and the floating ground signal is adjusted with both the coarse and fine zero potentiometers, and is fed back into the square signal. The coarse zero pot is used to bring the balance across the null position, and the fine zero pot is used to adjust the voltage divider until it is matched to the square signal.

The slew rate, or the rate of change of the voltage of the square signal, is varied with the slew rate switch that selects a combination of capacitors from a capacitor bank. The slew rate is adjusted so that the maximum voltage swing of the square signal is never reached. As a first order approximation, this new signal is the integral or the continuous area of the square signal, which is directly related to the mass change of a sample in the microbalance.

The new restoring signal is finally sent to the compensating coil where it is combined with the out-of-

phase damping signal to restore the balance to the null position. The restoring signal is also sent to a strip chart recorder for display.

A change in mass of the sample produces a deflection in the beam, which causes the symmetry of the square signal to be altered. When the altered signal is integrated, the change in area of the square signal above and below the zero point is reflected in the restoring signal, which represents the change in mass. This change in the restoring signal is then sent to the coil to bring the deflected beam back to the null position.



## APPENDIX C: PROPOSED DIGITAL CONTROLLER

The microbalance controller used in this study is extremely limited. It is an analog instrument with a floating ground which makes it extremely sensitive to electrical noise. It requires a great deal of time and patience to keep running properly, and it has no way of monitoring experiments other than sending the output to a recorder. In order to correct these problems, a computer controlled digital microbalance controller is proposed.

A digital controller would be capable of monitoring such things as when the equilibrium of an adsorption run is reached. The system could be programmed to analyze the data as they are produced to give information such as the rate of adsorption. Once a sample is loaded into the balance, an entire experiment could be run from a keyboard, or, if expanded to control valves, the system could control an entire series of experiments.

### Hardware

The circuit diagram of the proposed circuit is shown in Figure C-1. The proposed circuit combines circuitry from part of the analog microbalance controller, along with some digital circuitry, and is a variation of the work done at an earlier date (12) with a potential improvement to the sensibility.

I R Detector Bridge. The infrared detector bridge circuit is the same one that is being used on the balance with the analog controller. The bridge detects a deflection in the beam and sends an error signal to the amplifier A1.

Amplifier A1. A1 is an inverting amplifier that amplifies the incoming error signal to about  $\pm 200$  millivolts, following the equation  $V_2/V_1 = -R_2/R_1$ . The signal is then split and sent to A2 in the damping circuit and A7 in front of the digital circuit.

Amplifier A2. Amplifier A2 is used as in the analog controller to differentiate the error signal into an out-of-phase signal to attenuate the response of the beam to the restoring signal. S1 is closed when the beam crosses the null position for the first time to begin damping the motion of the beam.

Amplifier A7. Amplifier A7 is an inverting amplifier that amplifies the signal to  $\pm 5$  volts, following the equation  $V_3/V_2 = -R_{10}/R_9$ . At  $\pm 5$  volts, the signal is compatible with the A/D (analog to digital) converter.

Digital Circuit. The error signal enters the digital circuitry through a 16 bit A/D converter where the error signal becomes a 16 bit word that is passed through a PIA (periferal interface adapter) into a personal computer. The computer then processes the data with software and

sends a restoring signal back to the rest of the circuit. The computer's signal passes back through the PIA to a 16 bit DAC (digital to analog converter). The output of the DAC is an analog signal of 19.5 millivolts per step and is sent to the attenuator A6.

Attenuator A6. The attenuator A6 reduces the DAC output of 19.5 millivolts per step to 0.05 millivolts per step, following the equation  $V_7/V_6 = -R_{12}/R_{11} = .00256$  . This signal, which is compatible with the operation of the microbalance, is sent to the adder at A3.

Adder A3. The adder uses the amplifier A3 to add the compensating signal from A6 and the damping signal from A2, following the equation  $-V_5/R_8 = V_7/R_7 + V_4/R_5$  . The signal is then sent to the voltage follower at A4 which acts as a buffer. The final compensating signal is then sent to the restoring coil, where the voltage range will be -6.4 mV to 1.2864 volts with a step size of .05 mV.

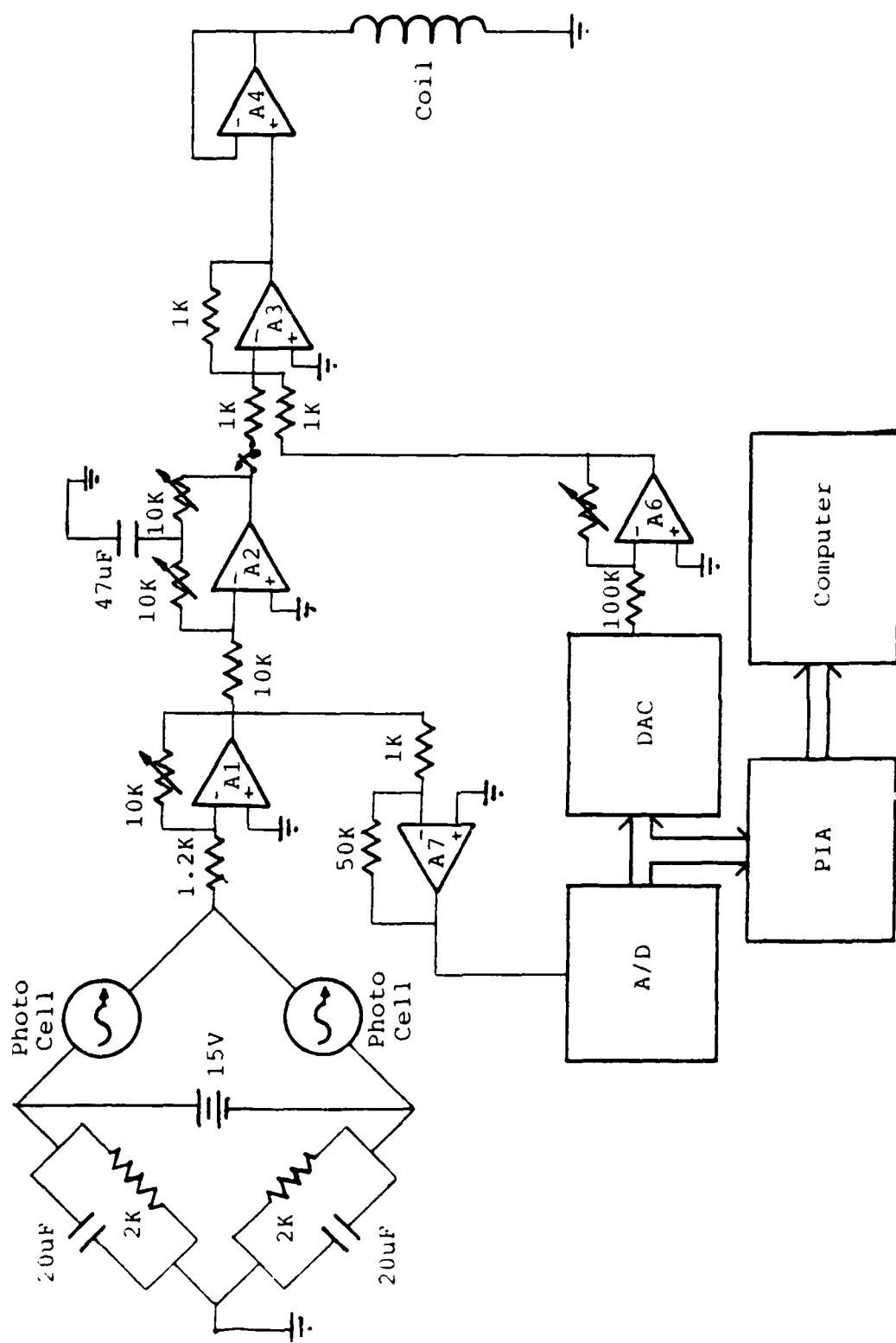


Figure C-1. Proposed Digital Microbalance Controller.

#### APPENDIX D: BET SURFACE AREA MEASUREMENT

The following is the step-by-step method of determining the surface area of a sample that has undergone gravimetric adsorption testing. The Brunauer, Emmett and Teller (BET) surface area technique described here was assembled from Robens (21:159), Czanderna (5:194), and Czanderna and Vasofsky (10:49).

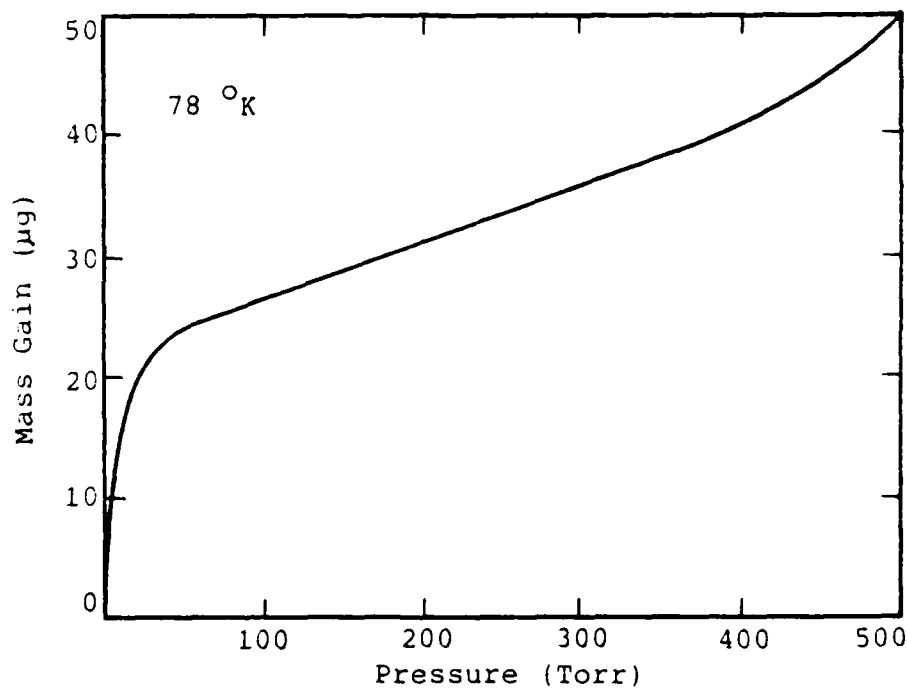


Figure D-1. Adsorption Isotherm of Nitrogen  
Adsorbed on Silver Powder. (10:49)

1. The first step is to obtain an adsorption isotherm with at least three points between the partial pressures of



0.05 and 0.35  $p/p_0$ , where  $p$  is the pressure of the adsorbate and  $p_0$  is the vapor pressure of the adsorbate gas at the isothermal temperature. An example is shown in Figure D-1.

2. The two parameter BET equation is a straight line and is given by

$$X / ((1-X)m) = ((C-1)/m_m C) X + 1/m_m C \quad (1)$$

where

$X$  =  $p/p_0$   
 $m$  = mass of adsorbed gas  
 $m_m$  = mass of adsorbed gas for monolayer coverage  
 $C^m$  = BET constant

3. The next step is to replot the isotherm between .05 and .35  $p/p_0$  as  $X / ((1-X)m)$  v.s.  $X$  to obtain a straight line with slope  $S$  and positive intercept  $I$ . If these conditions are not met, the BET analysis is not valid. The new plot of the isotherm in Figure D-1 is shown in Figure D-2.

4. Substituting  $S$  and  $I$  into equation (1) yields

$$X / ((1-X)m) = SX + B \quad (2)$$

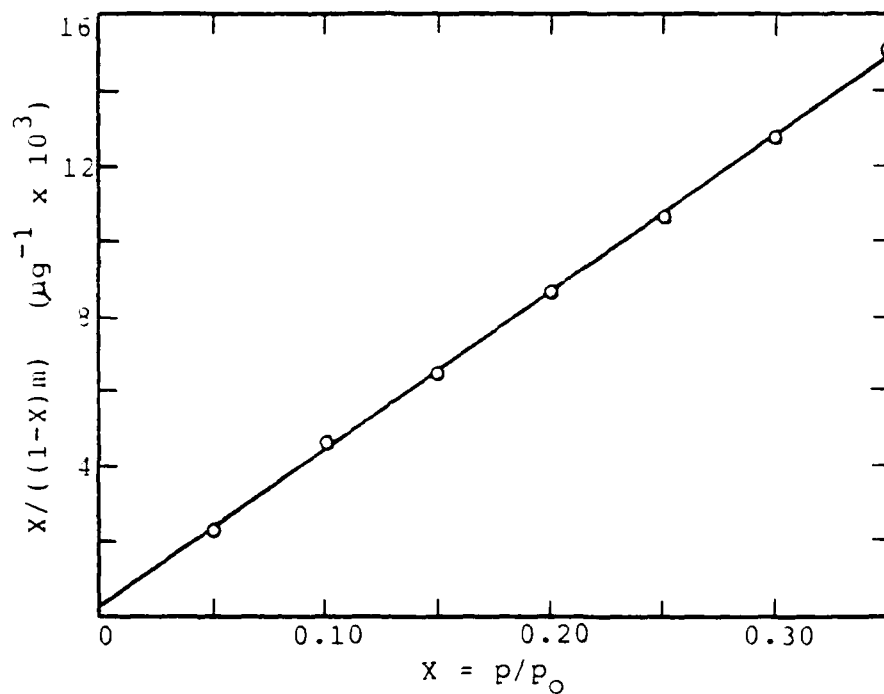


Figure D-2. BET Plot of Nitrogen Adsorbed on Silver Powder. (10:49)

where

$$S = (C-1)/m_m C \quad (3)$$

and

$$I = 1/m_m C \quad (4)$$

Solving for C in equations (3) and (4), and setting them equal gives

$$C = 1/m_m I = 1/(1-m_m S) \quad (5)$$

Solving for the mass of a monolayer coverage of molecules in equation (5) gives  $m_m$

$$M_m = 1/(S+I) \quad (6)$$

AD-A151 893 THE EFFECTS OF WATER AND HYDROGEN ON MATERIALS USED IN  
INTEGRATED CIRCUIT PACKAGES(U) AIR FORCE INST OF TECH  
WRIGHT-PATTERSON AFB OH SCHOOL OF ENGI. M W PRAIRIE  
UNCLASSIFIED DEC 84 AFIT/GE/ENG/84D-51 F/G 11/9

THE EFFECTS OF WATER AND HYDROGEN ON MATERIALS USED IN  
INTEGRATED CIRCUIT PACKAGES(U) AIR FORCE INST OF TECH  
WRIGHT-PATTERSON AFB OH SCHOOL OF ENGI.. M W PRAIRIE  
DEC 84 AFIT/GE/ENG/84D-51 F/G 11/9

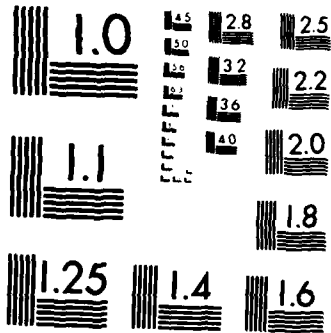
MI

UNCLASSIFIED

DEC 84 AFIT/GE/ENG/84D-51

F/G 11/9

END



MICROCOPY RESOLUTION TEST CHART  
NATIONAL BUREAU OF STANDARDS-1963 A

5. The specific surface area can now be calculated by using

$$A_s = (m_m A_m N_A) / (M m_s (1000)) \quad (7)$$

where

$A_s$  = specific surface area ( $m^2/g$ )  
 $m_m$  = adsorbate mass for monolayer coverage (g)  
 $A_m$  = cross-sectional area of adsorbed molecule ( $m^2$ )  
 $N_A$  = Avagadro's number ( $6.02 \times 10^{23}$  1/mole)  
 $M$  = gram molecular weight of adsorbate (g/mole)  
 $m_s$  = mass of the sample (g)

Robins (21:157) gives the value of  $W_g$  for nitrogen as 3480, where  $W_g = A_m N_A / M$  ( $m^2/g$ ). For the information in figure D-2,  $m_m = 23.5$  micrograms, and  $m_s = .7414$  grams,  $A_s = .00011$   $m^2/g$  of silver powder.

## APPENDIX E: MICROBALANCE PARTS LEGEND

The following is a legend of the parts of the microbalance system shown in Figure III-1 (28:712).

- (A) Balance Housing
- (B) Quadrupole Mass Filter
- (C) Turbomolecular Pump
- (D) Line to Gas Handling System
- (E) Leveling Platform
- (F) Support Table
- (G) Transite Top
- (H) Hangdown Tubes
- (I) Alignment Bolts
- (J) Solenoid Assembly
- (K) Solenoid Support Flange
- (L) Windows
- (M) "Y" Fitting with Port
- (N) Motor-driven Linear Motion Feedthrough
- (O) Sample Loading Fitting
- (P) Quick Access Flange
- (Q) Four-way Cross
- (R) Six-way Cross with Push-pull Feedthrough
- (S) Capacitance Manometer Gauge Tube
- (T) Tubulation for Pumping Reference Side of (S)
- (U) Straight Through Valves

- (V) "Tee" Fitting
- (W) Flexible Bellows
- (X) Manifold
- (Y) Vacuum Bakeout Oven
- (Z) Dry Box
- (AA) Uncoupling Point for Sample Suspension Fibers
- (BB) Bellows
- (CC) Location for Changing Sample and then Taring  
after Resuspending Sample
- (DD) Access Doors to Vacuum Bakeout Oven
- (EE) Vacuum or Backfilling Line
- (FF) Tube Furnaces

## BIBLIOGRAPHY

1. Bond, G. C. Catalysis by Metals. New York: Academic Press, 1962.
2. Bruck, Stephen D. "Thermogravimetric Studies on an Aromatic Polyimide in Air and in the Vacuum Region of  $10^{-2}$  to  $10^{-3}$  Torr Using the Cahn RG Electrobalance," Vacuum Microbalance Techniques, Volume 4, edited by Paul M. Waters. New York: Plenum Press, 1965.
3. Cahoon, J. R. and R. Bandy. "Auger Electron Spectroscopic Studies on Oxide Films of Some Austenitic Stainless Steels," Corrosion, 38(6): 299-305 (June 1982).
4. Cutting, P. A. and N. D. Parkyns. "Use of Vacuum Microbalances for Determining Physical Adsorption Isotherms of Vapors on Solids," Journal of Vacuum Science Technology, 13(1): 543-548 (January/February 1976).
5. Czanderna, A. W. "Chemisorption Studies with the Vacuum Microbalance," Microweighing in Vacuum and Controlled Environments, edited by A. W. Czanderna and S. P. Wolsky. New York: Elsevier Scientific Publishing Company, 1980.
6. Czanderna, A. W. "The Measurement of Adsorption and Desorption of Gasses from Solid Surfaces," Ultra Micro Weight Determination in Controlled Environments, edited by S. P. Wolsky and E. J. Zdanuk. New York: John Wiley and Sons, Inc., 1969.
7. Czanderna, A. W. "Thermodesorption Studies with a Vacuum Microbalance," Vacuum Microbalance Techniques, Volume 6, edited by A. W. Czanderna. New York: Plenum Press, 1967.
8. Czanderna, A. W. and J. M. Honig. "Sensitive Quartz Beam Microbalance," Analytical Chemistry, 29(8): 1206-1210 (August 1957).
9. Czanderna, A. W., et al. "Photoelectrically Automated, Bakeable, High-load Ultramicrobalance," Journal of Vacuum Science Technology, 13(1): 556-559 (January/February 1976).
10. Czanderna, A. W. and R. W. Vasofsky, "Surface Studies with the Vacuum Microbalance," Progress in Surface Science, Volume 9, edited by S. Davidson. Great Britain: Pergamon Press Ltd., 1979.



11. Czanderna, A. W. and S. P. Wolsky. "Introduction and Microbalance Review," Microweighing in Vacuum and Controlled Environments, edited by A. W. Czanderna and S. P. Wolsky. New York: Elsevier Scientific Publishing Company, 1980.
12. Donham, Sergeant Perry C., Lab Technician, Product Evaluation Section. Personal Interview. RADC/RBRE, Griffiss AFB NY, 8 March 1984.
13. Granville Philips Company. Instruction Manual. 275118001. Boulder CO, undated.
14. Henderson, Douglas and Ian K. Snook. "Adsorption of Gasses and Vapors on a Solid Surface," Journal of Physical Chemistry, 87(15): 2956-2959 (1983).
15. Hussey, R. J. et al. "A Bakeable Vacuum Microbalance for Determining Metal Oxidation Kinetics," Journal of Vacuum Science Technology, 11(1): 397-399 (January/February 1974).
16. Irbe, Ivars, Product Evaluation Section. Personal correspondence. RADC/RBRE, Griffiss AFB NY, 13 September 1984.
17. Kollen, W. and R. Vasofsky. "Simultaneous Micro-gravimetric and Residual Gas Analyzer Measurements," Microweighing in Vacuum and Controlled Environments, edited by A. W. Czanderna and S. P. Wolsky. New York: Elsevier Scientific Publishing Company, 1980.
18. Massen, C. H. and J. A. Poulis. "Cavity Forces, an Error in Adsorption Measurements," Vacuum Microbalance Techniques, Volume 6, edited by A. W. Czanderna. New York: Plenum Press, 1967.
19. Pierotti, Robert A. "Gas-Solid Interactions and Buoyancy," Vacuum Microbalance Techniques, Volume 6, edited by A. W. Czanderna. New York: Plenum Press, 1967.
20. Rasmussen, M. D. and M. Akinc. "Microcomputer-Controlled Gravimetric Adsorption Apparatus," Review of Scientific Instrumentation, 54(11): 1558-1564 (November 1983).
21. Robens, E. "Physical Adsorption Studies with the Vacuum Microbalance," Microweighing in Vacuum and Controlled Environments, edited by A. W. Czanderna and S. P. Wolsky. New York: Elsevier Scientific Publishing Company, 1980.

22. Romeo, Glauco, et al. "Computerized Digital Data Aquisition System for Thermogravimetry and Similar Applications," Analytical Chemistry, 45(14): 2444-5 (December 1973).
23. Schwobel, R. L. "Beam Microbalance Design, Construction and Operation," Microweighing in Vacuum and Controlled Environments, edited by A. W. Czanderna and S. P. Wolsky. New York: Elsvier Scientific Publishing Company, 1980.
24. Sienko, M. J. and R. A. Plane. Chemistry: Principals and Applications. New York: McGraw-Hill Book Company, 1979.
25. Swartz, W. E., et al. "The Adsorption of Water on Metallic Packages," Proceedings of the 21st Symposium on Reliability Physics. 52-59. IEEE Press, New York, 1983.
26. Thomas, J. H. III and S. P. Sharma. "Adsorption and Desorption of Water on Au by the Quartz Crystal Oscillator Method," Journal of Vacuum Science Technology, 13(1): 549-551 (January/February 1976).
27. Thomas, John M. and Brian M. Williams. "Application of a Metal Vacuum Microbalance to the Study of Solid Surfaces by Physical Adsorption," Vacuum Microbalance Techniques, Volume 4, edited by Paul M. Waters. New York: Plenum Press, 1965.
28. Vasofsky, R., et al. "UHV System for the Ultramicrogravametric Study of Samples Loaded in a Controlled Environment," Journal of Vacuum Science Technology, 16(2): 711-14 (March/April 1979).
29. Uthe Technology International. UTI 100 C Precision Mass Analyzer. Operating and Service Manual. Sunnyvale CA, 1972.

## VITA

Second Lieutenant Michael W. Prairie was born on 16 September 1961 in Holyoke, Massachusetts. He graduated from South Hadley High School in South Hadley, Massachusetts, in 1979 and attended Norwich University in Northfield, Vermont. There, he studied for a degree in electrical engineering while holding several positions in the Norwich University Corps of Cadets over the four year period. He graduated with honors and received the degree of Bachelor of Science in Electrical Engineering in May 1983. Upon graduation, he received a commission in the USAF through the ROTC program. He was immediately called to active duty and entered the School of Engineering, Air Force Institute of Technology, in June of 1983.

Permanent address: 13 Grant Street

South Hadley, Massachusetts 01075

UNCLASSIFIED

SECURITY CLASSIFICATION OF THIS PAGE

## REPORT DOCUMENTATION PAGE

1. REPORT SECURITY CLASSIFICATION <b>UNCLASSIFIED</b>			1b. RESTRICTIVE MARKINGS	
2a. SECURITY CLASSIFICATION AUTHORITY			3. DISTRIBUTION/AVAILABILITY OF REPORT  Approved for public release, distribution unlimited.	
2b. DECLASSIFICATION/DOWNGRADING SCHEDULE				
4. PERFORMING ORGANIZATION REPORT NUMBER(S)  AFIT/GE/ENG/84D-51			5. MONITORING ORGANIZATION REPORT NUMBER(S)	
6a. NAME OF PERFORMING ORGANIZATION  School of Engineering		6b. OFFICE SYMBOL (If applicable) AFIT/ENG		7a. NAME OF MONITORING ORGANIZATION
6c. ADDRESS (City, State and ZIP Code)  Air Force Institute of Technology Wright-Patterson AFB, Ohio 45433			7b. ADDRESS (City, State and ZIP Code)	
8a. NAME OF FUNDING/SPONSORING ORGANIZATION  Dr. Robert W. Thomas Product Evaluation Section		8b. OFFICE SYMBOL (If applicable) RADC/RBRE		9. PROCUREMENT INSTRUMENT IDENTIFICATION NUMBER
8c. ADDRESS (City, State and ZIP Code)  Rome Air Development Center Griffiss AFB, New York 13441			10. SOURCE OF FUNDING NOS.	
11. TITLE (Include Security Classification)  See Box 19			PROGRAM ELEMENT NO.	
			PROJECT NO.	
12. PERSONAL AUTHOR(S)  Michael W. Prairie, B.S.E.E., 2d Lt, USAF			TASK NO.	
			WORK UNIT NO.	
13a. TYPE OF REPORT  MS Thesis		13b. TIME COVERED FROM _____ TO _____		14. DATE OF REPORT (Yr, Mo., Day)  1984 December 3
15. PAGE COUNT  102				
16. SUPPLEMENTARY NOTATION				
17. COSATI CODES			18. SUBJECT TERMS (Continue on reverse if necessary and identify by block number)	
FIELD	GROUP	SUB GR	Gravimetric Analysis, Microbalance, Vacuum, Ultrahigh Vacuum, Adsorption, Water Adsorption, Packaging Materials Polyimide, Gold, Nickel	
11	06			
11	09			
19. ABSTRACT (Continue on reverse if necessary and identify by block number)				
<p>Title: THE EFFECTS OF WATER AND HYDROGEN ON MATERIALS USED IN INTEGRATED CIRCUIT PACKAGES</p> <p>Thesis Chairman: Donald R. Kitchen, Captain, USAF</p> <p>Abstract: This investigation determined the adsorption properties of water on RC-5878 polyimide, rolled gold foil, and rolled nickel foil at 20°C, as well as the effects that hydrogen has on nickel foil with a monolayer coverage of water molecules. Adsorption isotherms were obtained using a vacuum ultramicrobalance with a sensibility of 0.1 micrograms per 10 gram load. The microbalance system includes a gas handling system, a thermal conductivity cell, and a quadrupole residual gas analyzer. The isotherms were analyzed using the B. E. T. surface area technique. (Continued.)</p>				
20. DISTRIBUTION AVAILABILITY OF ABSTRACT  UNCLASSIFIED UNLIMITED <input checked="" type="checkbox"/> SAME AS RPT. <input type="checkbox"/> OTIC USERS <input type="checkbox"/>			21. ABSTRACT SECURITY CLASSIFICATION  UNCLASSIFIED	
22a. NAME OF RESPONSIBLE INDIVIDUAL  Donald R. Kitchen, Captain, USAF			22b. TELEPHONE NUMBER (Include Area Code)  (513) 255-4960	22c. OFFICE SYMBOL  AFIT/ENG

Approved for public release: IAW AFR 190-17,  
LTCN E. W. WILSON, 21 Feb 85  
Dean for Research & Professional Development  
Air Force Institute of Technology (AFIT)  
Wright-Patterson AFB OH 45443

19. (Cont'd) The results showed that RC-5378 polyimide adsorbs water in an amount proportional to the thickness of the sample when the given cure is used. The rolled gold foil showed no mass gain from water adsorption. The nickel foil adsorbed water on 0.86 cm<sup>2</sup> of the 210 cm<sup>2</sup> sample, and adsorbed on 0.40 cm<sup>2</sup> during the second run of the experiment. An Auger scan revealed a large concentration of oxygen due to nickel oxide, which acted as a passivation layer for the remaining nickel sample surface. A monolayer of water molecules was obtained on the nickel surface, and hydrogen was admitted to the system. The sample exhibited a mass gain which was attributed to hydrogen bonding on the nickel oxide surface.

**END**

**FILMED**

**5-85**

**DTIC**